NASA CR 111935

QUASI-STEADY AND SHORT PULSE DISCHARGE THRUSTER EXPERIMENTS

by

William J. Guman

June, 1971

PCD-TR-71-3, FHR 3795-1, PC004R7001

Prepared under Contract NAS1-9925
Fairchild Industries, Inc.
Fairchild-Republic Division
Farmingdale, New York 11735

for

National Aeronautics and Space Administration
LANGLEY RESEARCH CENTER
Langley Station
Hampton, Virginia 23365

NASA CR 111935

QUASI-STEADY AND SHORT PULSE DISCHARGE THRUSTER EXPERIMENTS

by

William J. Guman

June, 1971

PCD-TR-71-3, FHR 3795-1, PC004R7001

Prepared under Contract NAS1-9925
Fairchild Industries, Inc.
Fairchild-Republic Division
Farmingdale, New York 11735

for

National Aeronautics and Space Administration
LANGLEY RESEARCH CENTER
Langley Station
Hampton, Virginia 23365

FOREWORD

This final report summarizes the work performed under contract NAS 1-9925 for National Aeronautics and Space Administration, Langley Research Center, Hampton, Virginia. The effort was accomplished under the direction of Mr. J. M. Hoell of NASA, Langley.

Dr. W. J. Guman was the principal investigator. Mr. M. Begun performed the dynamic impedance measurements and assisted in the design of the pulse forming network. The laboratory effort was performed with the assistance of Mr. M. Katchmar and the support of Messrs: E. Poggi and L. Odorico.

Besides these individuals, the stimulating discussions with Professor R. G. Jahn of Princeton University are gratefully acknowledged.

ABSTRACT

The solid teflon propellant pulsed plasma thruster was scaled to operate in the millipound thrust regime. The performance of the thruster was determined and compared when operated either as a short pulse discharge thruster or as a quasi-steady thruster. Erosion was also quantitatively evaluated. The performance of propellant breech fed short pulse discharge thruster configurations scaled predictably into the millipound regime from earlier microthruster results. Exploratory tests with propellant side-feed configurations showed significant performance improvements could be realized over breech fed configurations. A power to thrust ratio of 156 watts/milli-lb was measured at a specific impulse of 1245 sec. Erosion was found to depend upon electrode material and the duration of the test. In particular, erosion expressed as the ratio of mass eroded to propellant mass used was found to vary directly with specific impulse. When erosion is expressed as the ratio of mass eroded to total impulse delivered, this erosion parameter is also found to have a slight dependence upon specific impulse.

The somewhat limited number of results show thrust efficiency of short pulse discharge operation to be better than quasi-steady operation when compared at the same specific impulse. Erosion measured during short pulse discharge operation was found to be much lower than that measured for quasi-steady discharge operation compared at the same specific impulse.

CONTENTS

ILLUSTRATIONS

ILLUSTRATIONS (Cont'd)

SECTION I

INTRODUCTION

Previous studies of either short pulse discharge thrusters or quasi-steady thrusters have been treated as separate studies. The work to be described compares the propulsive performance and erosion behavior of an accelerator nozzle assembly when it is operated either as a short pulse discharge thruster or as a quasi-steady thruster. Unlike most previous quasi-steady thruster studies the discharge energy used in the present studies was kept at a level compatible with auxiliary propulsion requirements. Furthermore, the present study was limited to the use of solid teflon as the propellant. Such a solid propellant thruster eliminates gas propellant injection valves, electric switches, and the timing circuit required to match propellant flow to the electric discharge. The practicality of the solid propellant approach has been established[1] by more than two and one-half years of operation in space. The thruster used in the latter flight application was a microthruster. The present study required that thruster operation be first scaled from the former micropound thrust regime to the millipound thrust regime yet retaining a specific impulse in the range from 1000 to 3000 sec. After the short pulse discharge thruster was successfully scaled to operate in the millipound thrust regime the dynamic impedance of its arc was used to design the pulse forming network required for quasi-steady operation.

Propulsive performance and erosion were quantitatively determined for both short pulse and quasi-steady operation with comparable initial discharge energies. The scope and duration of the program limited the number of data points obtained. While the present results show short pulse thruster operation to be better than comparable quasi-steady thruster operation, it is important not to consider the present results as conclusive proof that short pulse operation is generally superior to quasi-steady operation. It is hoped the present results will suggest future studies of a similar nature to provide more data over a wider range of operating parameters.

SECTION 2

MEASUREMENT AND EVALUATION TECHNIQUES

2.1 THRUST AND IMPULSE BIT

The thrust levels presented are the directly measured thrust obtained by mounting the entire thruster and its solid propellant feed system on a Republic designed and built thrust balance. Figure 1 shows the quasi-steady thruster mounted on the thrust balance in the vacuum test chamber. The vacuum chamber is 6 feet in diameter and 8 feet long. Chamber pressure during thruster operation is typically 10^{-4} mm Hg. Calibration of the thrust balance is performed just prior to measuring thrust without disturbing the vacuum or the thruster during thruster performance tests.

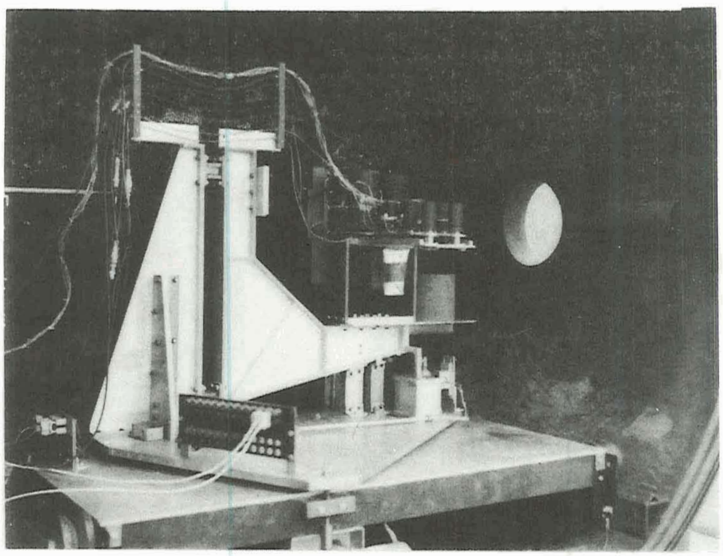

Figure 1. Quasi-Steady Thruster on Thrust Balance in Vacuum Chamber

The thrust balance is a "soft" thrust measuring stand and has been described in detail elsewhere.[2] The thrust is measured directly. The impulse bit of each discharge is calculated from the relation

$$\text{Impulse bit amplitude} = \frac{\text{measured thrust}}{\text{pulse frequency of operation}}$$

with the pulse frequency measured during a run by using a stop watch to time the elapsed time of from 30 to 60 consecutive pulses. Thrust measurements are recorded from four to six times during a typical diagnostic test of several hours of thruster operation. This technique provides a significant amount of data to assess thruster performance and also allows any temporal performance changes, if present, to be recorded. The thrust and impulse values presented are the test average values recorded during the entire period of operation. Generally small variations observed during a run are either statistical in nature or are due to small variations in applied voltage and are within the general accuracy of the measurement of about ±5%. The repeatability of test results can best be demonstrated by using data generated during final erosion studies where test conditions were repeated a number of times in order to obtain erosion data as a function of consecutive discharges. Table 1 presents data of 7 repeated tests and the ratio of test average applied voltage, measured test average specific impulse and measured test average impulse bit to the respective mean value of the 7 tests. The data illustrates that deviations from the respected mean values are well within ±5% with most of the data being within ±2% from the mean value.

Both the calibration and thrust readings are permanently recorded on a Sanborn recorder. Figure 2 presents a view of the test equipment exterior to the vacuum test chamber.

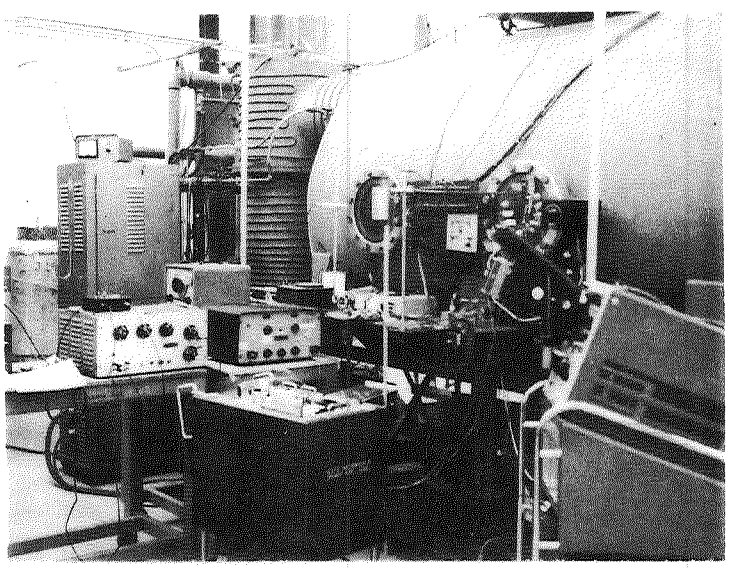

Figure 2. Typical Test Equipment Exterior to Vacuum Chamber

TABLE 1. Repeatability of Test Results

TEST DATA						Deviation from Test Series Mean Value		
Test	# Shots	V, Volts	f, Hz	I_{sp} Sec	I, μ lb Sec	V/V_m	$I_{sp}/I_{sp\,m}$	I/I_{mean}
131x1	10,000	2356	1.006	1575	1213.2	0.9937	1.0101	0.9478
131x4	20,000	2406	1.000	1518	1262	1.0148	0.9736	0.9859
131x5	20,000	2437	1.000	1600	1344.3	1.0279	1.0262	1.0502
131x6	20,000	2346	0.996	1545	1260	0.9895	0.9909	0.9843
131x7	20,000	2337.5	1.004	1580	1303	0.9859	1.0134	1.0179
131x8	20,000	2343	0.997	1568	1297	0.9882	1.0057	1.01328
131x9	20,000	2370	0.993	1528	1281	0.9996	0.9800	1.0007
Mean Value		2370.8		1559.1	1280.0			

2.2 MASS MEASUREMENT

Mass measurements were made on propellant consumption and anode, cathode and insulator assembly erosion. For purposes of evaluating thruster performance propellant mass measurements are those performed on the weight change of initially stored solid propellant mass. These latter measurements are performed by measuring the weight change of the initially stored solid teflon propellant rod before and after operating the thruster a given number of discharges. The propellant rod is measured to the nearest 0.2 milligram on a Christian Becker style AB-8 analytic balance. This balance has a capacity of 2 kg. The quantity of propellant mass consumed per thruster discharge is calculated from the relation

$$\text{Propellant mass per discharge} = \frac{\text{Total propellant mass change}}{\text{Total number of thruster discharges}}$$

The number of thruster discharges are recorded by a counter. It is important to note that the latter quantity of propellant mass per discharge is based upon the weight change of stored propellant mass per thruster discharge. This latter parameter enables a meaningful propulsion system propellant specific impulse to be calculated. Diagnostic measurements for determining mass utilization efficiency were not carried out. While such diagnostic measurements are useful for determining the percent of propellant mass that can be attributed to the impulse bit delivered, they are extremely difficult to perform and are outside the scope of the present studies.

2.3 EROSION

Electrode and insulator erosion were measured in the same manner as propellant mass changes. The anode, cathode and insulator assembly of a thruster were weighed before and after thruster operation. The mass change per discharge of these subcomponents is calculated as described in Section 2.2. Since quasi-steady thruster operation could only be carried out with the anode permanently sealed to the discharge circuit it was not possible to make anode erosion measurements during quasi-steady thruster operation.

After performing a diagnostic test the thruster was allowed to cool to room temperature while soaking in a vacuum (of the order of 10^{-5} mm Hg). This soaking period usually lasted about 15 hours. This procedure was adopted to prevent significant mass changes due to surface effects.[3]

2.4 CURRENT AND VOLTAGE

Discharge current was measured by using a calibrated Rogowsky coil. The discharge voltage was measured by using two Tektronix P6013 high voltage probes and connecting one to each of the two electrodes. The cathode was used as the common ground. The output of the two probes was recorded on a Type G wide band differential amplifier in a 551 Tektronix Oscilloscope. The zero voltage reference line was obtained by removing voltage from the capacitor bank and remotely switching a dead short across the two electrodes.

2.5 PERFORMANCE PARAMETERS

Several operational and thruster performance parameters were determined. These include:

a. Stored capacitor energy: This energy is calculated from the relation

$$E = 1/2\ CV^2$$

with C the measured capacitance and V the initial voltage (just prior to a discharge) on the capacitor as measured with the voltage probes described in Section 2.4.

b. Delivered energy: Due to capacitor and discharge circuit losses not all of the stored capacitor energy is delivered to the accelerator nozzles. The electric energy actually delivered is determined by evaluating the integral:

$$E_d = \int E(t)\ i(t)\ dt$$

with E(t), i(t) the instantaneous terminal discharge voltage and instantaneous discharge current, respectively. This latter integral is evaluated graphically using a polar planimeter.

c. Impulse Bit: The impulse bit per discharge is calculated as described in Section 2.1.

d. Thrust: The thrust is the thrust measured directly by a thrust balance as described in Section 2.1.

e. Propellant mass: The propellant mass per discharge is the change in initially stored solid propellant mass used per thruster discharge and measured as described in Section 2.2.

f. Total mass per discharge: The total mass per thruster discharge is comprised of the sum of the propellant mass per discharge plus the total eroded mass per discharge. Unless otherwise noted, the eroded mass includes anode, cathode and insulator erosion.

g. Propellant specific impulse: This parameter is calculated from any one of the relations:

$$I_{sp_p} = \frac{\bar{T}}{\bar{\dot{w}}} = \frac{\bar{T}n}{\bar{f}w_t} = \frac{\bar{I}}{\bar{w}}$$

where $\bar{T}$, $\bar{\dot{w}}$, $\bar{f}$, w_t, n, $\bar{I}$, $\bar{w}$ denote test average thrust, test average propellant weight flow rate, test average pulse frequency, stored propellant weight change for an entire test, total number of discharges of test, test average impulse bit, test average stored propellant weight change per discharge, respectively. As mentioned in Section 2.2, the propellant specific impulse as calculated above, provides the most meaningful specific impulse for propulsion system analysis.

h. Total mass specific impulse: This specific impulse (I_{sp_t}) is calculated by also including the eroded mass. Since no attempt was made in the present study to determine either material or electrode nozzle configurations having the least erosion, the total mass specific impulse is presented to illustrate the range of performance that may be quoted for a given set of test data when erosion is included.

i. Thrust efficiency: Generally it is understood that this parameter is given by the expression:

$$\eta = \frac{T^2}{2 \dot{m} P}$$

with T, $\dot{m}$, P the thrust, propellant mass flow rate and electric power, respectively. Depending upon whether one is interested only in basic mass acceleration processes or only in propulsive system aspects, one can evaluate thrust efficiency in any of a number of ways. This latter possibility is due to the fact that for diagnostic purposes one may be interested only in the propellant mass actually used in the acceleration process, or in the power actually transferred into the propellant accelerated. For propulsion system considerations one may be interested only in the quantity of power and propellant mass that must be supplied to the propulsion system. To avoid ambiguities in the experimental data presented in this study, thrust efficiency will, on occasion, be calculated and presented as four different sets of numbers. This latter presentation will be useful when comparisons are made between short pulse and quasi-steady thruster operation. In such cases, the notation to be used will clearly define the thrust efficiency calculated.

For a pulsed plasma thruster the above definition of thrust efficiency may be rewritten in the form

$$\eta = \frac{I^2}{2 m E}$$

with I, m, and E the impulse bit per discharge, the quantity of propellant mass per discharge and the energy per discharge respectively. It is important to note that the specific impulse and thrust efficiency of each single discharge of a given plasma thruster configuration are the same as are determined when the thruster operates repetitively at a pulse frequency f.

The four calculations of thrust efficiency that may be presented in this study are as follows: (in all cases the impulse bit is the value measured as discussed in Section 2.1):

1. $\eta = \eta\,(E_s, m_p)$ with (E_s) the energy initially stored in the capacitor and (m_p) the change in stored propellant mass per discharge. This calculated efficiency will generally be of interest for propulsion system considerations. Furthermore, unless otherwise denoted, the symbol η will always denote $\eta\,(E_s, m_p)$ in this study.

2. $\eta = (E_d, m_p)$ where the energy (E_d) is the quantity of electric energy delivered to the accelerator nozzle (see Section 2.4), and m_p the change in stored propellant mass per discharge.

3. $\eta = (E_s, m_t)$ where the energy (E_s) is the energy initially stored in the capacitor and m_t the total mass, i.e., propellant mass plus eroded mass per discharge.

4. $\eta = (E_d, m_t)$ where the energy (E_d) is the delivered energy and m_t the total mass, i.e., propellant mass plus eroded mass per discharge.

While the limited number of different electrode material that was selected and tested was believed to represent material having a low level of erosion, it is possible that other material not evaluated during the present study could have a lower level of erosion compared to the ones examined. Furthermore, electrode configurations examined are not based upon configurations having the lowest level of erosion. The performance data presented which includes mass lost by erosion could possibly be different for different material or different electrode configurations.

SECTION 3

SHORT PULSE THRUSTER

3.1 DESIGN

The short pulse discharge pulsed plasma thruster used during the present studies uses solid teflon as the propellant. The accelerator nozzle assembly is configured as a parallel rail electrode nozzle and is coupled to the capacitors to form a series LCR circuit. A schematic representation of the thruster is shown in Figure 3.

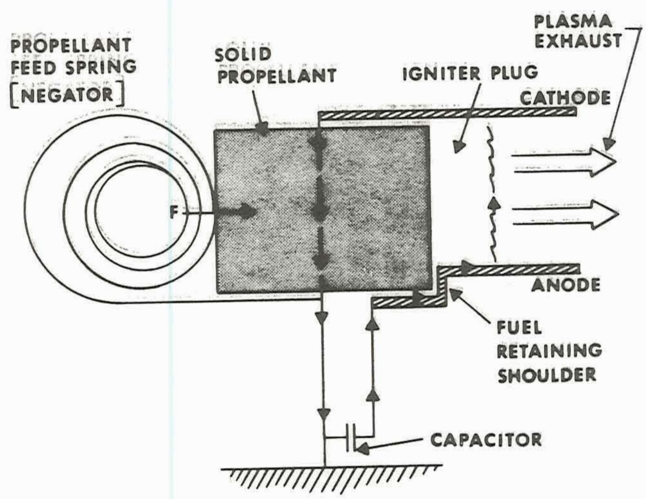

Figure 3. Thruster Schematic

The terminals of the energy storage capacitor are connected by a low inductance, low resistance path to the anode and to the cathode of the thruster accelerator nozzle, respectively. A fuel retaining shoulder is machined into the anode in order to properly position the teflon propellant rod with respect to the thruster nozzle. A constant force steadily provided by a Negator spring assures that an edge of the propellant is held against the fuel retaining shoulder.

The capacitor bank utilized energy storage capacitors from an earlier program. The number of capacitors and their rating could easily be varied during the program. While a relatively low inductance discharge circuit was used, no attempt was made to minimize total circuit inductance to the lowest possible value.

Conceptually, many of the features of the short pulse discharge thruster of the present program resemble features of the solid teflon pulsed plasma microthruster.[1] As with the microthruster, a simple Negator spring is used to feed the propellant during thruster operation. Figure 4 shows a rear view of the thruster. The twelve energy storage capacitors as well as the teflon propellant rod and its feed spring can be seen. Figure 5 shows the front view of the thruster with an open sided parallel rail nozzle having a large propellant area fed from the breech end of the nozzle. The propellant rod, anode, cathode and insulator assembly can be easily removed in order to perform measurements of their weight change. Figure 6 shows these four subcomponents after their removal from the thruster. The insulator assembly is fabricated of Mykroy, the cathode of 17-7 ph stainless steel, and the anode of tungsten on a 17-7 ph stainless steel substrate, respectively. During a special erosion test series both the anode and cathode set were fabricated of sets of 17-7 ph stainless steel, molybdenum and 2% thoriated tungsten, respectively. With the exception of this latter erosion test series and the molybdenum test series, the same set of electrodes and insulators were used for all performance tests. During these diagnostic performance tests the electrodes and insulator were cleaned and weighed before and after each test.

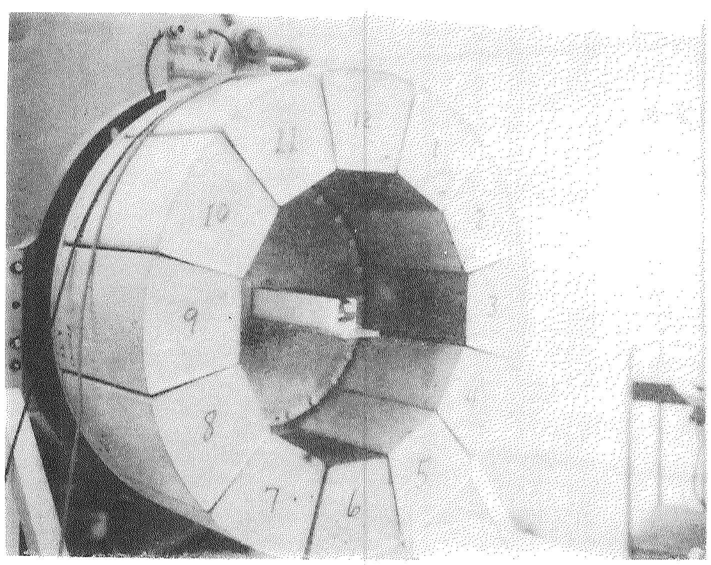

Figure 4. Rear View of Short Pulse Discharge Thruster

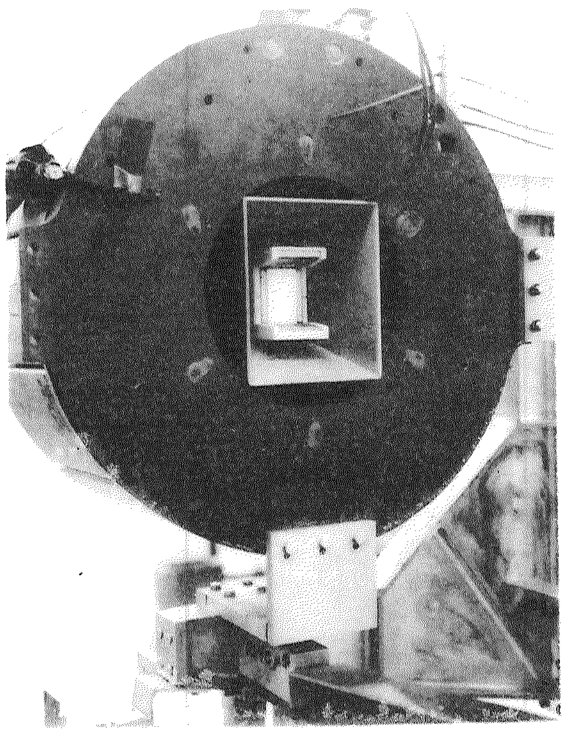

Figure 5. Front View of Short Pulse Discharge Thruster

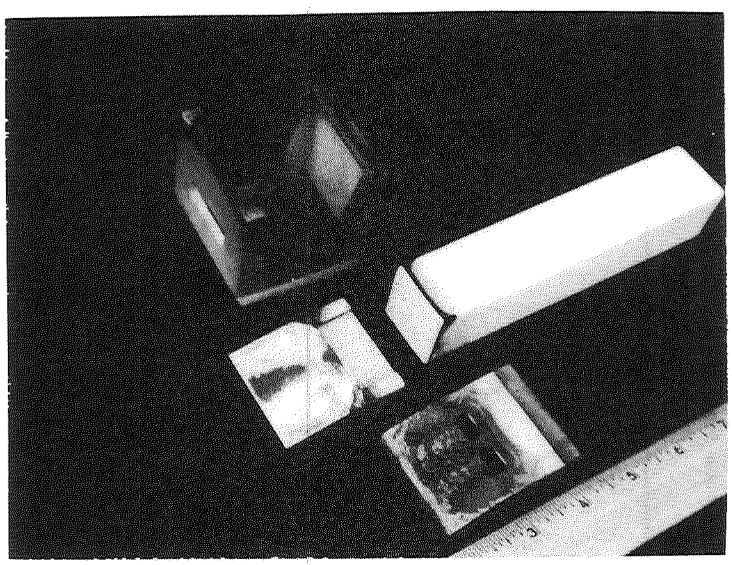

Figure 6. Insulator, Anode, Cathode and Propellant Rod of Short Pulse Thruster After Typical Performance Test

Most of the performance tests were performed with propellant supplied to the discharge from the breech end of the accelerator nozzle such as shown in Figure 5. Toward the end of the program a few exploratory tests were performed in which the propellant was supplied simultaneously from the breech end as well as the downstream sides of the discharge. Two of the latter exploratory propellant configurations include V-shaped propellant rod and a breech-plus-side-feed configuration. Figure 7 presents a schematic representation of these latter configurations. These new propellant configurations increase the propellant flow rate to the discharge more effectively than breech fed configurations thereby significantly increasing the thrust/power ratio compared to breech-fed configurations.

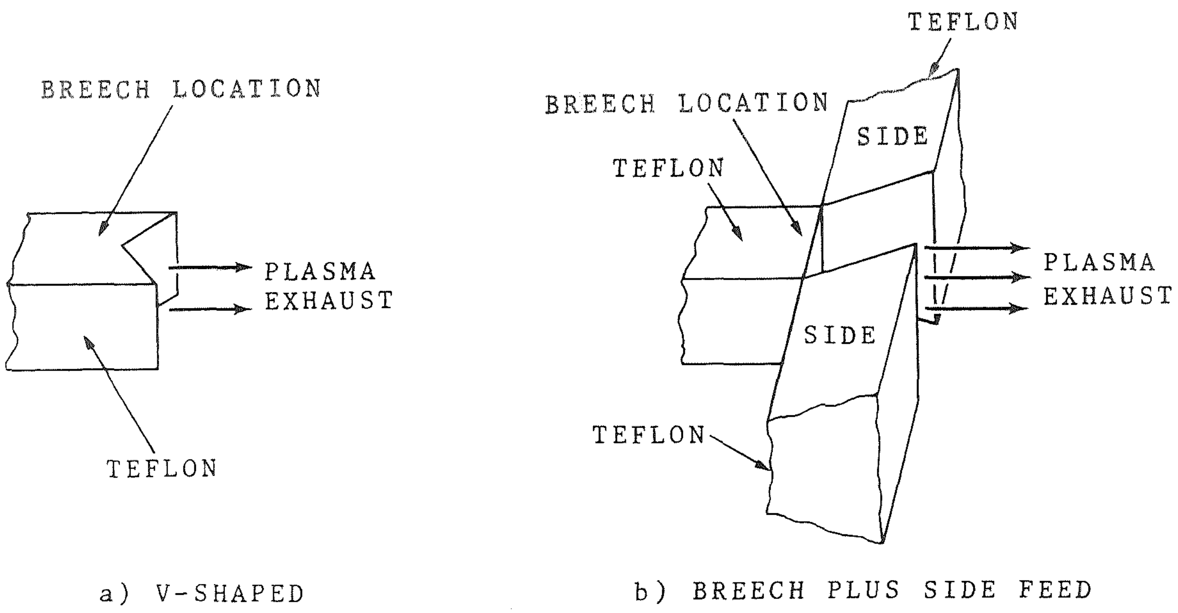

Figure 7. Propellant Side-Feed Geometries

3.2 EXPERIMENTAL RESULTS

3.2.1 Performance

Table 2 presents a summary of the performance data obtained with the short pulse discharge thruster. Because of the relative ease by which capacitors, propellant rods and electrode nozzles could be incorporated and tested in the basic short pulse discharge thruster shown in Figures 4 and 5, a number of tests were performed before the quasi-steady thruster was available for testing. For convenience in comparing the test results obtained, the data in Table 2 is presented in four major columns:

- I Breech fed configuration, fixed propellant area of 1.69 in^2, varying discharge energy
- II Breech fed configuration, fixed propellant area of 2.94 in^2, varying discharge energy
- III Breech plus-side-fed configuration, varying propellant area, nearly constant discharge energy
- IV V-shaped propellant.

The first horizontally grouped data in Table 2 provides details of test conditions. The second group presents propulsive system performance data. The third horizontal grouping presents the performance data including energy losses in delivering the capacitor energy to the thruster nozzle and also mass losses due to erosion. This latter data therefore reflects the quality of the particular set of energy storage capacitors used and also the suitability of electrode and insulator material used in the thruster.

Figure 8 presents thrust efficiency $\eta\ (E_s, m_p)$ as a function of propellant specific impulse using the nine data points in the second horizontal grouping of Table 2. Also presented are data points of breech-fed microthrusters.[4] The discharge energy of these latter thrusters range from about 1 to 20 joules with impulse bit levels varying from about 3 μ lb-sec to about 100μlb-sec. The results presented in Figure 8 show that the solid propellant breech fed short pulse discharge plasma thruster scaled in a predictable manner from the micropound to the millipound thrust regime. As with the microthruster, the present large energy results of breech fed configurations also operated at a thrust/power ratio (I/E_s) of about 4 milli-lb/kw. This value was increased about 50% by also introducing propellant into the discharge from the sides, downstream of the breech. The data in the last two vertical columns of Table 2 present this latter performance improvement that was realized. Similar results have also been obtained with propellant side-fed microthrusters.[5] The three experimental

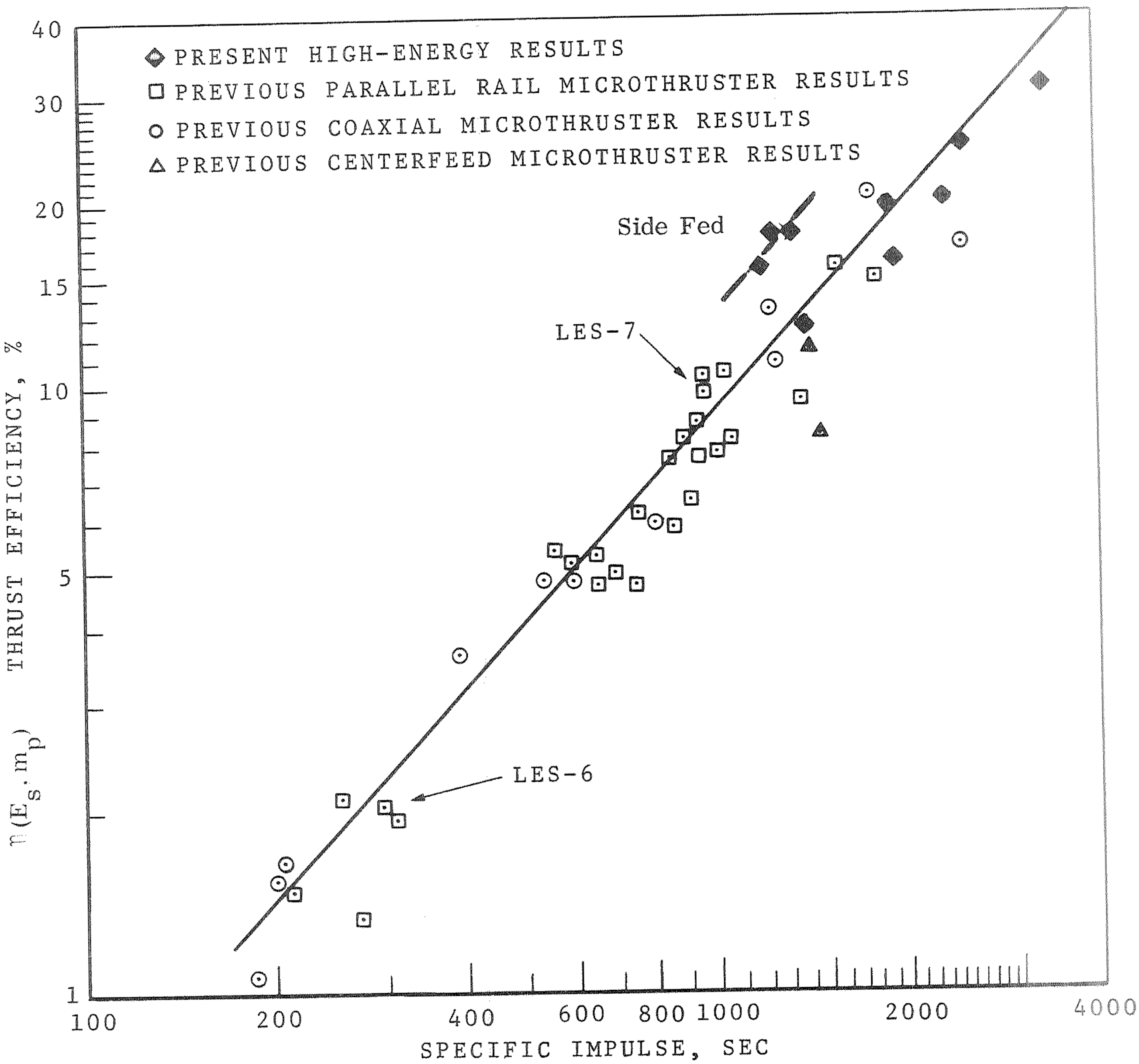

Figure 8. Thrust Efficiency $\eta(E_s, m_p)$ as a Function of Propellant Specific Impulse for Short Pulse Discharge Thruster

TABLE 2. Experimental Data of Short Pulse Discharge Thruster Operation

	I				II		III		IV
Capacitor Energy, E_s, Joules	171	318	358*	452	171	318	461	486	526
Propellant area, in^2	1.69	1.69	1.69	1.69	2.93	2.93	5.51	9.13	8.28
Capacitance, μfd	282.2	282.2	114.5	114.5	282.2	282.2	114.5	114.5	114.5
Initial Voltage, kv	1.1	1.1	2.5	2.8	1.1	1.5	2.84	2.91	3.03
Shots of test	9286	8035	2567	7688	9178	8171	7674	7938	6754
Pulse frequency, Hz	0.957	0.969	0.531	0.572	0.977	0.971	0.532	0.531	0.538
Test duration at f, Hrs.	2.69	2.3	1.34	3.74	2.61	2.33	4.0	4.15	3.5
Test avg. thrust, μlb	625	1240	790	1147.6	680	1482.5	1454.4	1645.6	1694.6
Impulse bit, I, μ lb-sec	652	1280	1485	2000	695	1528	2735	3100	3140
Propellant specific impulse, sec	1900	2240	3330	2500	1400	1900	1328	1245	1160
Thrust efficiency η (E_s, m_p), %	15.8	19.7	30.2	24.2	12.4	19.85	17.2	17.4	15.1
Thrust/pwr ratio (I, E_s), mlb/kw	3.84	4.03	4.15	4.43	4.06	4.8	5.93	6.39	5.975
Pwr/thrust ratio (E_s, I), w/m lb	261	248	241	226	246	208	168.5	156.5	167.
Delivered energy, E_d, joules	165.8	271	---	---	162	251	420	---	---
Engy Trnsfr eff, E_d/E_s, %	0.97	0.853	---	---	0.948	0.79	0.91	---	---
Total mass spec. impulse, sec	1800	2070	2880	2300	1350	1838	1295	1230	1145
Thrust eff. η (E_d, m_p), %	16.3	23.1	---	---	13.1	26.0	18.8	---	---
Thrust eff. η (E_s, m_t), %	14.95	18.25	26.1	22.2	11.95	19.2	16.8	17.2	14.9
Thrust eff. η (E_d, m_t), %	15.4	21.4	---	---	12.6	25.1	18.4	---	---
Thrust/pwr ratio, (I, E_d), m lb/	3.93	4.72	---	---	4.29	6.08	6.5	---	---
Power/thrust ratio (E_d, I), w/mlb	255	212	---	---	233	164.5	154	---	---
Log	121x5	121x6	121x14	121x12	121x7	121x8	121x13	121x15	121x17
I_{sp}/I_{sp_t}	1.053	1.081	1.153	1.088	1.037	1.032	1.023	1.011	1.011
η (E_s, m_p)/η (E_s, m_t)	0.97					1.032	1.022	1.01	1.01
*carbon filled teflon									

data points of the side-fed configuration are not described by the same straight line data trend line shown in Figure 8. The higher side-fed thrust/power ratio data points fall along another data trend line rotated counterclockwise with respect to the trend line that describes the performance of breech fed thrusters.

To interpret the information contained in Figure 8, it should be remembered that a pulsed plasma thruster delivers discrete impulse bits of amplitude I. The specific impulse (I_{sp}) and efficiency (η) of a single impulse are then:

$$I_{sp} = I/mg$$

$$\eta = I^2/(2mE)$$

With the impulse bit/energy ratio given by I/E and the quantitiy of propellant mass per discharge denoted by m, the specific impulse and efficiency of the pulsed plasma thruster can be presented without involving the concept of thrust or electric power. These latter quantities become meaningful only when a given thruster is operated at some pulse frequency f. In cases of repetitive operation one finds the specific impulse, efficiency and thrust/power ratio of steady state operation at a pulse frequency f to be numerically equal to the corresponding values of each single discharge and independent of pulse frequency, as seen from the following relations:

$$I_{sp} = T/\dot{W} = f\ I/f\ W = I/W$$

$$\eta = T^2/2\dot{m}p = I^2/2mE$$

$$T/P = I/E$$

Hence the performance of a given thruster appears as a single data point on a plot of η versus I_{sp} (Figure 8) independent of its power level or thrust level of operation. The thrust level of a given thruster is varied merely by changing pulse frequency. The thrust level (or power level) can thus be varied over a very wide range at constant I_{sp} and η. The specific impulse and efficiency of a pulsed plasma thruster are varied by changing parameters other than pulse frequency. For example:

a. Changing applied voltage for otherwise fixed conditions
b. Changing capacitance for otherwise fixed conditions
c. Changing thruster electrode nozzle geometry
d. Changing the quantity of propellant consumed per discharge

or any combination of these.

Table 2 also presents the results of performance calculations which include capacitor losses and mass losses due to erosion. These results show the range of performance that may be quoted for a given set of test data if such effects are included. Caution must be exercised in making generalized conclusions from these latter results which include erosion. Since the same set of electrodes were used during all of the performance tests, the rate of erosion encountered during any given test was not only a function of the particular test conditions of that test, but also of the prior history of the electrodes. This latter effect will be discussed in more detail in Section 3.2.2 which presents erosion data obtained by repeating a given set of test conditions with a given set of electrodes. Furthermore, it will also be shown that the selection of electrode material can substantially affect erosion and therefore also affect any performance figures quoted which include the effect of erosion.

While for practical applications it is important to reduce loss mechanisms to an absolute minimum, the effect of loss mechanisms on the general range of performance of the short pulse discharge thrusters examined has in most cases not been too important. The performance of a given short pulse discharge thruster is sufficiently well described (i.e., to within a few percent) by the propellant specific impulse and the thrust efficiency η (E_s, m_p). It is perhaps interesting to note that not only do the side feed geometries examined provide a higher thrust/power ratio than the breech fed geometry, but also has the smallest change in performance due to erosion. This latter observation will be discussed in more detail in Section 3.2.2.

3.2.2 Erosion

Three test sets of erosion data were taken during the present study. The first set was taken during the short pulse discharge thruster and quasi-steady thruster performance evaluation tests. The same set of electrodes were repeatedly used being cleaned only between individual performance evaluation tests. The second set of tests examined erosion of three different electrode materials. For this test series three identical sets of electrodes were fabricated and subjected to the same test conditions. The third test series examined the change in erosion by subjecting a given set of electrodes repeatedly to the same test conditions. In no cases were electrode geometries sought for minimum erosion. The results of these three sets of tests will now be presented.

3.2.2.1 First Test Series: The first set of tests in which erosion data was taken were performed with a 17-7 ph stainless steel cathode and a tungsten anode mounted on a 17-7 ph stainless steel substrate. This set of electrodes was used during all of the thruster performance evaluation studies reported upon. The electrodes and insulator (see Figure 6 for a typical set) were weighed before and after each performance test. Table 3 presents the results of these tests. These include the short pulse discharge thruster tests of Table 2 and the quasi-steady thruster tests of Table 7. Erosion of the anode, cathode, insulator and combinations of these are presented as percent of teflon propellant consumed. Since the given set of electrodes is irreversibly minutely changed from test to test, the erosion data of the first test series is believed to be somewhat limited for quantitatively assessing erosion of a given set of test conditions. This statement is based upon the results of the third test series where it was found that erosion of a given set of electrodes repeatedly used under the same test conditions can give a pulse life dependent result.

In Reference 6 it was found that for a given electrode material the quantity of eroded mass dependend primarily upon the charge q passing between the electrodes. The present short pulse discharge thruster results do not show a correlation between erosion expressed in grams/discharge with the charge q. Malliarus[7] recently has shown erosion for a quasi-steady thruster to depend upon molecular weight and the parameter $i^2/\dot{m}$ with i and $\dot{m}$ the discharge current and propellant mass flow rate, respectively. The simplified analyses presented below shows the parameter $i^2/\dot{m}$, rewritten in terms of the mean of the square of the current, to be directly related to the specific impulse. The simplified analyses is therefore also suitable for encompassing data of short pulse thrusters.

TABLE 3. Erosion Data of Diagnostic Test Series

a) Short Pulse Thruster Data

Log	121x5	121x6	121x14	121x12	121x7	121x8	121x13	121x15	121x17
Propellant I_{sp}, sec	1900	2240	3330	2500	1400	1900	1328	1245	1160
$m_{anode}/m_{prop}/$, %	4.0	6.05	3.84	6.79	2.23	2.98	0.51	0.437	0.396
m_{cath}/m_{prop}, %	0.1245	0.4048	1.49	0.988	0.358	0.0805	1.71	0.746	0.427
m_{insul}/m_{prop}, %	1.188	1.298	8.45	0.952	1.23	0.1735	0.092	+0.0379	0.0624
Total erosion, %	5.31	7.75	13.78	8.73	3.82	3.23	2.31	1.145	0.88
$m_{cath+ins}/m_{prop}$, %	1.31	1.7	9.94	1.94	1.59	0.25	1.80	0.71	0.49
m_{c+i}/Imp., lb/lb-sec	6.9×10^{-6}	7.84×10^{-6}	3×10^{-5}	7.75×10^{-6}	1.128×10^{-5}	1.34×10^{-6}	1.36×10^{-5}	5.69×10^{-6}	4.23×10^{-6}
m_{ca-a+i}/Imp, lb/lb-sec.	2.79×10^{-5}	3.49×10^{-5}	4.13×10^{-5}	3.48×10^{-5}	2.72×10^{-5}	1.7×10^{-5}	1.74×10^{-5}	0.92×10^{-5}	0.765×10^{-5}

b) Quasi-Steady Thruster Data

Log	128x1	128x2	128x3	128x4
Prop. Spec. Imp, sec	3070	2680	1340	975
m_{anode}/m_{prop}	---	---	---	---
m_{cath}/m_{prop}	---	7.11	4.68	4.76
m_{insul}/m_{prop}	---	28.7	1.4	1.0
$m_{cath+ins}/m_{prop}$	---	35.81	6.08	5.76
m_{c+i}/Imp. lb/lb-sec	---	13.3×10^{-5}	4.53×10^{-5}	5.9×10^{-5}

Since specific impulse was measured for all performance tests presented in Table 2, Figure 9 presents erosion as a function of propellant and total mass specific impulse respectively. Even though the data encompasses different initial conditions and slightly varying geometry from test to test due to erosion, the correlation between total erosion (expressed in percent of propellant mass) and either total mass or propellant specific impulse is considered reasonably good.

$$\frac{i^2}{\dot{m}} \propto \frac{\overline{i^2}}{\overline{\dot{m}}} = \frac{\frac{1}{\tau}\int_0^\tau i^2 dt}{\frac{1}{\tau}\int_0^\tau \dot{m} dt} = \frac{\frac{1}{\tau} i^2 dt}{m/\tau} = \frac{\int i^2 dt}{m}$$

Suppose we now assume the propulsive action to be entirely electromagnetic in origin. Then the instantaneous force F_i due to magnetic pressure P_m will be

$$F_i = P_m A = \frac{B^2 A}{2\mu}$$

Now the magnetic flux density B can be written as

$$B = Ki^2$$

with K some constant depending upon electrode geometry. The impulse bit I due to the ejection of a quantity of mass m is then

$$I = \int F_i \, dt = KA \int i^2 dt$$

But the specific impulse I_{sp} is:

$$I_{sp} = \frac{1}{g} \frac{I}{m} = \frac{1}{g} KA \frac{\int i^2 dt}{m}$$

Thus a direct relation is observed between the parameter

$$i^2/\dot{m} \quad \left(\propto \frac{\int i^2 \, dt}{m} \right) \text{ and specific impulse}$$

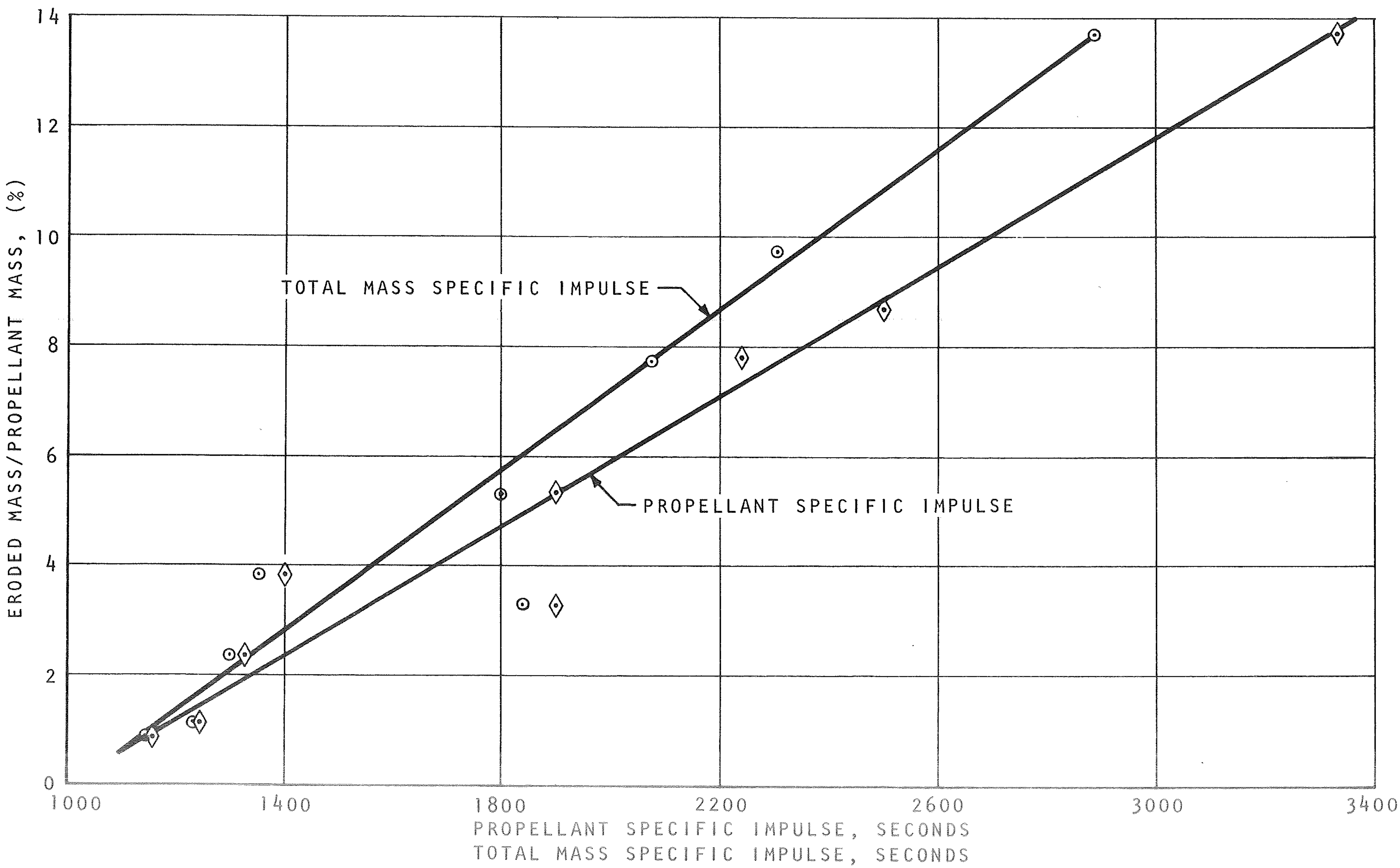

Figure 9. Percent Total Erosion as a Function of Propellant Specific Impulse and Total Mass Specific Impulse (Short Pulse Discharge Thruster)

At first glance, the erosion trend as observed in Figure 9 would suggest prohibitive erosion with increasing specific impulse. For practical applications, one is generally interested in delivering a certain total impulse over a given mission time. As the specific impulse is increased for a given total impulse the required quantity of propellant mass decreases. This trend is not reflected by presenting the data in the form of Figure 9. Figure 10 (also see Table 3) presents the quantity of eroded mass per unit total impulse (i.e., lb/lb-sec) as a function of specific impulse. From this latter figure it is seen that when specific impulse is varied from about 2200 to 3300 sec, the rate of erosion, expressed as lb/lb sec, increases only by about 18% compared to an increase of 77% as inferred from Figure 9 where erosion is expressed as percent of propellant weight. The lowest rate of erosion (lb/lb-sec) was found in the 1200 sec specific impulse range.

Since no attempt was made to evaluate electrode configurations or to seek for the electrode material that provides the lowest possible erosion, the above results must be considered valid only for the conditions tested. For example, the results of the second and third test series will demonstrate that electrode material as well as repeated use of a given electrode under the same test conditions can change any general conclusions one may infer from the data of the first test series. The effect of electrode geometry on erosion was beyond the scope of this study.

3.2.2.2 Second Test Series: Three identical sets of electrodes fabricated of 17-7 ph stainless steel, molybdenum and 2% thoriated tungsten were each discharged for 10,000 consecutive discharges. An attempt was made to maintain applied voltage and pulse frequency the same. The pulse frequency was maintained at 1Hz and discharge energy between 278 to 317 joules. Figure 11 shows the three sets of electrodes, the insulator assembly and the teflon propellant rod after each of the electrode sets was subjected to 10,000 consecutive discharges. It should also be observed that the teflon propellant remained quite flat during each run. The region of erosion of the anode appears as a light region. Table 4 presents the results of these tests. The data is also presented in Figure 10. The difference in erosion noted is attributed to differences in electrode material. These preliminary results suggest that proper selection of electrode material may reduce erosion considerably.

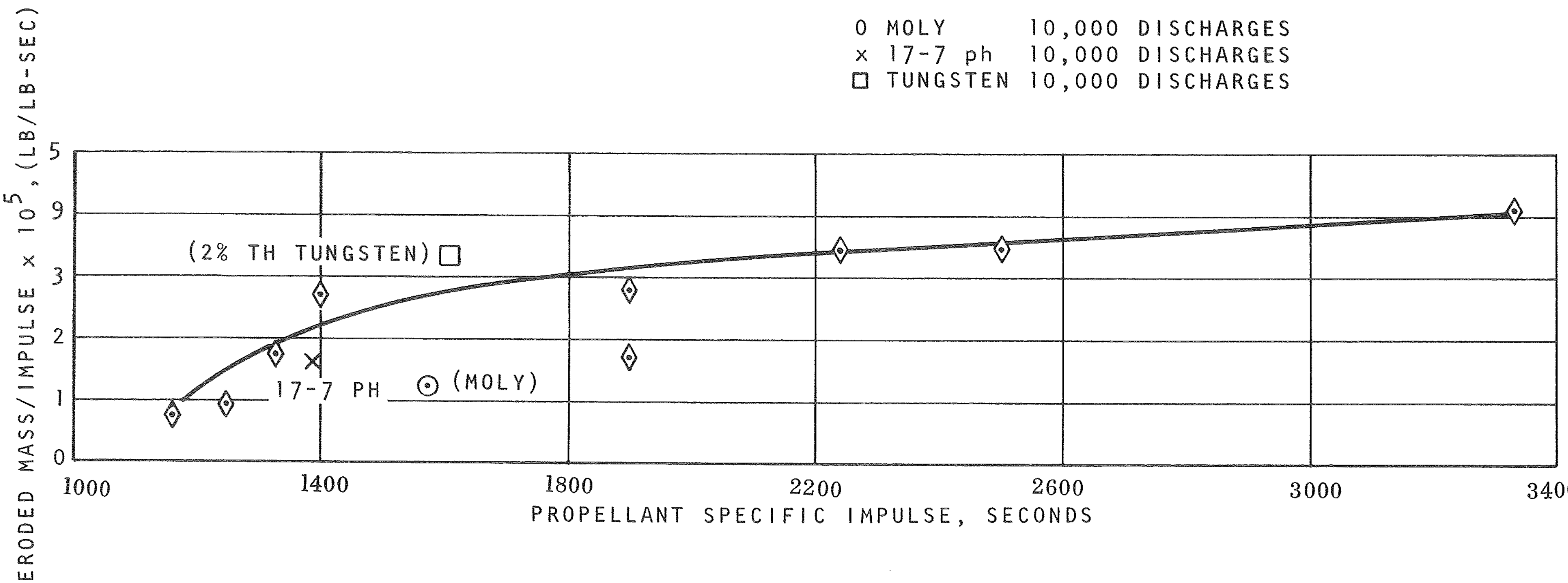

Figure 10. Eroded Mass per Unit Total Impulse as a Function of Specific Impulse

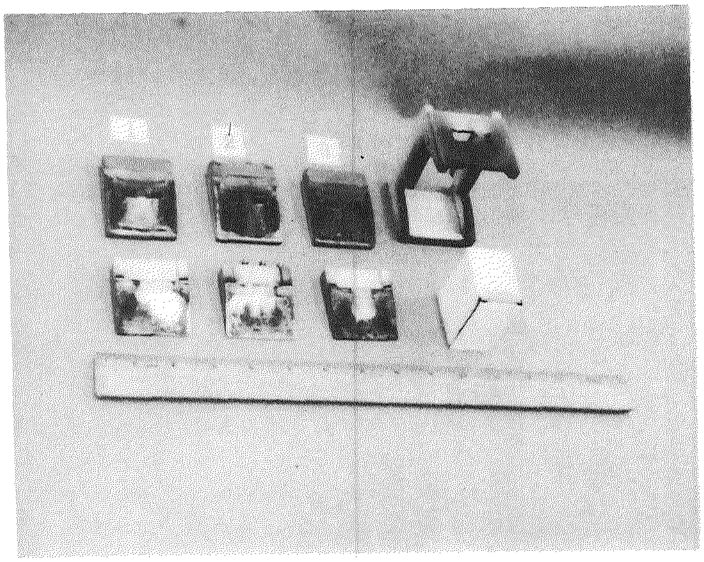

Figure 11. Electrode Sets After 10,000 Consecutive Discharges

1. Molybdenum
2. 17-7 ph Stainless Steel
3. 2% Thoriated Tungsten

Top Row - Cathodes
Lower Row - Anodes

The rates observed during the first test series and the results of the first test series presented in Table 2 are to be considered as preliminary results. Of the three electrode materials tested the 2% thoriated tungsten set showed the highest rate of erosion while the molybdenum electrodes experienced the least erosion.

TABLE 4. Electrode Material Erosion Studies (10,000 Consecutive Discharges)

Cathode Material	Molybdenum	17-7 ph stainless Steel	2% thoriated Tungsten
Anode Material	"	"	"
Anode weight loss/propellant wgt loss, %	1.35	1.483	4.83
Cathode wgt loss/propellant wgt loss, %	0.262	0.892	0.538
Insulator wgt loss/propellant wtg loss, %	0.337	+0.0617	0.0769
Anode, Cathode and insulator wgt/ propellant wgt loss, %	1.95	2.313	5.45
Mass loss eroded/Impulse, lb/lb-sec	1.235×10^{-5}	1.67×10^{-5}	3.38×10^{-5}
Discharge energy of test	327 j	278 j	304 j

Ducati compared the erosion of five different anode materials in his quasi-steady thruster studies.[8] Since no quantitative data was provided, it is not possible to compare his results with those reported herein. Of the five materials tested (aluminum, copper, molybdenum, tungsten, and graphite) Ducati notes that graphite experienced the smallest change in geometry due to erosion - graphite was followed by tungsten and then molybdenum. Certainly, besides the relative mass change due to erosion for practical applications it will also be necessary to consider the relative geometry change with time due to erosion such as observed by Ducati.

3.2.2.3 Third Test Series: During this test series the molybdenum electrodes were repeatedly subjected to the same test conditions. After operating the thruster for a prescribed number of consecutive discharges (20,000 - except the first test which was the 10,000 discharge test result of the second test series) the electrode, insulator and propellant were removed and weighed and without otherwise disturbing them, reinstalled for the next firing sequence. As with the first test series after each firing sequence the thruster assembly was allowed to return to room temperature while soaking overnight in an evacuated condition. Table 5 presents the results of this test series. The data is also presented in Figure 12. Figures 12a and 12b present erosion expressed as mass eroded/impulse and as percent of propellant mass as a function of consecutive discharges, respectively. Both figures show erosion essentially constant for about 20,000 consecutive discharges. Erosion was then found to become smaller as testing continued. Visual inspection of the electrodes showed that sharp corners and edges (see Figure 6) of the electrodes eroded faster than the flat surface of the electrode. It would be interesting to have tested Rogowsky electrodes[9] in which electric field effects are minimized.

The results of this erosion test show erosion to depend upon the number of consecutive discharges. Some caution must therefore be exercised in attributing erosion exclusively to operating parameters which do not include the duration of the test.

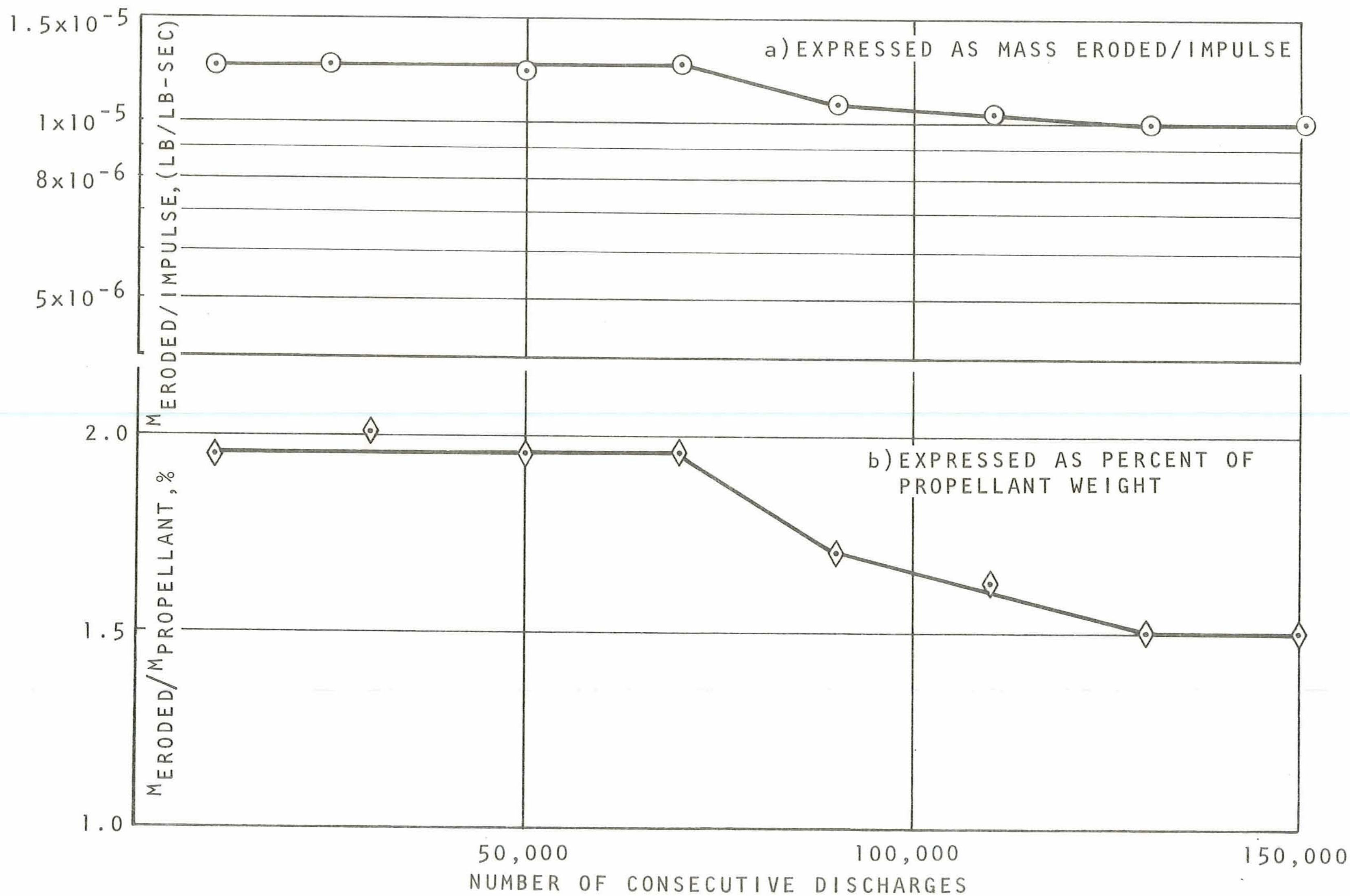

Figure 12. Erosion as a Function of Consecutive Discharges (Molybdenum Electrodes)

3.2.3 Parametric Studies

3.2.3.1 Impedance Considerations

Studies of the dynamic impedance of gaseous propellant thrusters have been reported by Michels.[10] Studies of the dynamic impedance variation of a 320 joule discharge teflon propellant thruster were performed during the current program by M. Begun. The discharge current and terminal voltage (iR drop and d/dt (Li) term) were displayed simultaneously on an oscilloscope. The thruster was operated steadily at about 1 Hz at initial capacitor voltages varying from about 200 volts up to 1500 volts. Discharge voltage and current traces were taken for these various initial voltages. The magnitude of instantaneous discharge voltage and current were subsequently determined at fixed times of 1, 2, 3, peak current, 5, 7, 9 and 10 μ sec from the various traces obtained for the different initial voltages. For each of these latter time values the instantaneous discharge voltage (corrected for the L di/dt term) was presented as a function of the corresponding discharge current. The dynamic impedance at each time was then determined from the slope $\Delta E/\Delta i$ of the voltage and current data points plotted for that time. These latter values of dynamic impedance were then replotted as a function of time from which they were evaluated. This latter technique provides more details on impedance behavior than that from the single point obtained by evaluating the dynamic impedance at peak current where the di/dt term vanishes. Figure 13 presents the variation in dynamic impedance. Except during the early part of the discharge, the dynamic impedance of the discharge of the teflon propellant thruster was found to be between 5 to 7 milliohms during most of the discharge. The pulse forming network was subsequently designed using a value of 6.5 milliohms as the arc impedance.

Assembling a thruster discharge circuit with a total initial impedance $\sqrt{Lo/c}$ of 5 to 7 milliohms is not an easy task. A technique was developed to readily facilitate an evaluation of the discharge circuit impedance at the instant the arc is initiated. This technique was found to be necessary since the shape of the arc at the instant it is initiated can affect the value of the initial inductance (and impedance) of the discharge circuit. This effect can be illustrated by some sample results. Table 6 presents discharge circuit parameters calculated from the ringing pattern obtained by shorting the circuit at the breech end of the thruster nozzle using two differently shaped "shorting bars". One shorting bar was in the shape of a flat plate simulating a plasma sheet

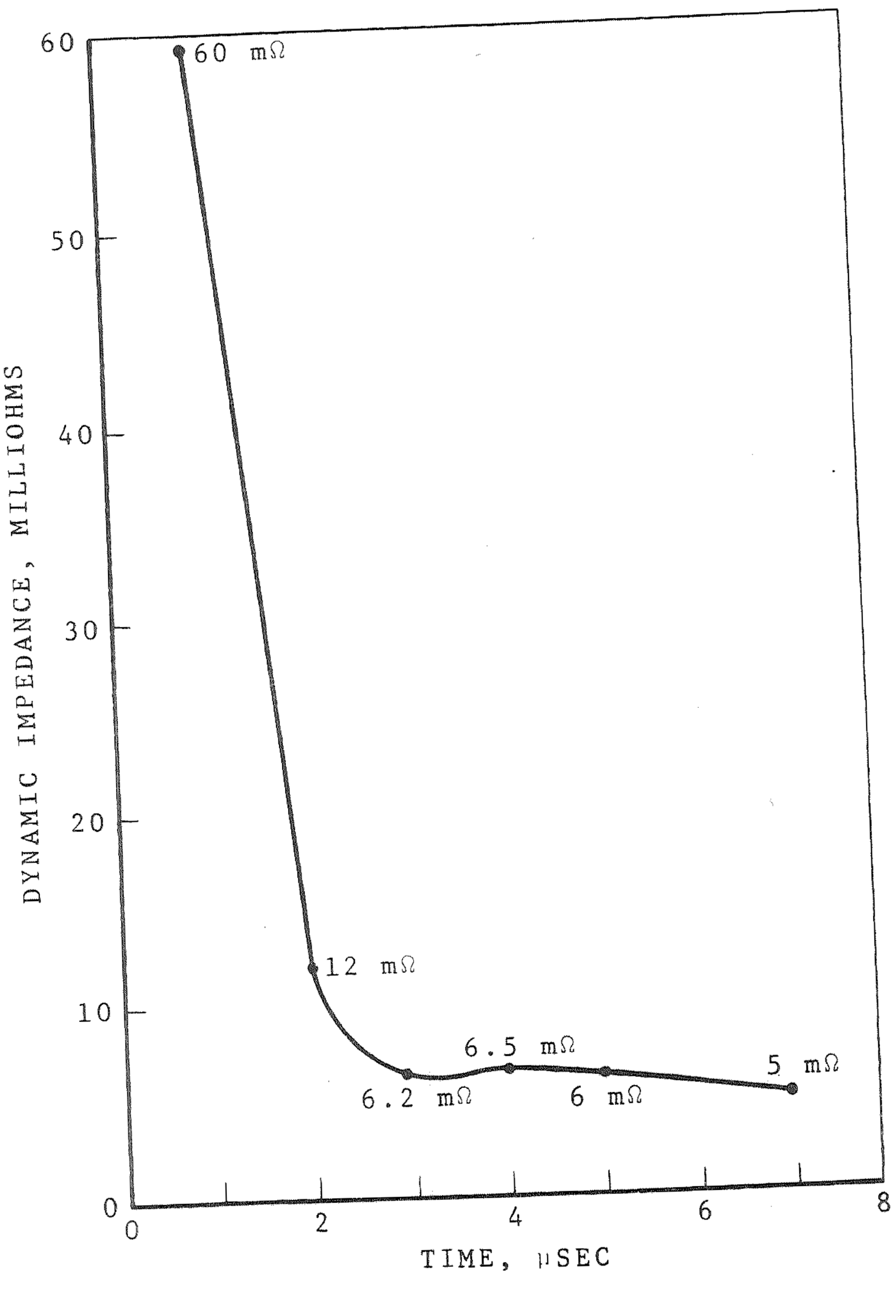

Figure 13. Dynamic Impedance as a Function of Time

TABLE 6. Initial Circuit Parameter Measurements

Shorting Configuration	Initial Inductance, H	Initial Impedance, Ohms
Flat plate	2.4×10^{-8}	9.21×10^{-3}
Thin wire	7.6×10^{-8}	16.4×10^{-3}
Initial arc (171 joules)	10.5×10^{-8}	19.3×10^{-3}
Initial arc (318 joules)	8.78×10^{-8}	17.6×10^{-3}

located at the breech of the nozzle. The second configuration was a thin wire simulating a line discharge at the breech of the nozzle. Also presented are experimental values of initial inductance and impedance obtained by operating the thruster at 171 joules and 318 joules, respectively. The inductance at the instant the thruster discharge is initiated was determined from the rate of change of discharge current with time at $t = 0$, i.e., from the relation $di/dt_{t=0} = Vo/Lo$ with Vo, Lo the initial voltage and inductance (including the plasma arc which closes the circuit at $t = 0$). This latter relation was shown by Andreev[11] to be valid for soft discharges. For such discharges the inductance is sufficiently large so that the voltage drop across the arc resistance can be neglected. For hard discharges, i.e., extremely low inductance circuits, the voltage drop across the arc cannot be neglected and the relation used is not valid. Thus for soft discharges (such as are presently encountered in the short pulse discharge thruster), the rate of energy release is governed by circuit inductance while arc resistance governs the rate of energy release for hard discharges. The discharge circuit impedance of the short pulse discharge thruster at arc initiation is thus $zo = \left[Vo/(c\, di/dt_{t=0})\right]^{1/2}$. The experimental data presented in Table 6 shows that the initial inductance and impedance of the thruster resembles a series LCR circuit in which the initial arc configuration resembles a thin wire (i.e., a line discharge). The lowest initial circuit impedance that has been measured with the available research thruster has been about 15×10^{-3} ohms. Studies are in progress to determine the design and the components to reduce this impedance to a level comparable to that of the arc during the time of mass acceleration.

3.2.3.2 Specific Impulse as a Function of Discharge Energy/Propellant Area Ratio

A correlation found useful in the design of short pulse discharge thrusters is the correlation of propellant specific impulse with discharge energy per unit propellant area being depolymerized[4]. Figure 14 presents the high energy short pulse discharge thruster data of the study including earlier low energy data of coaxial and rail type

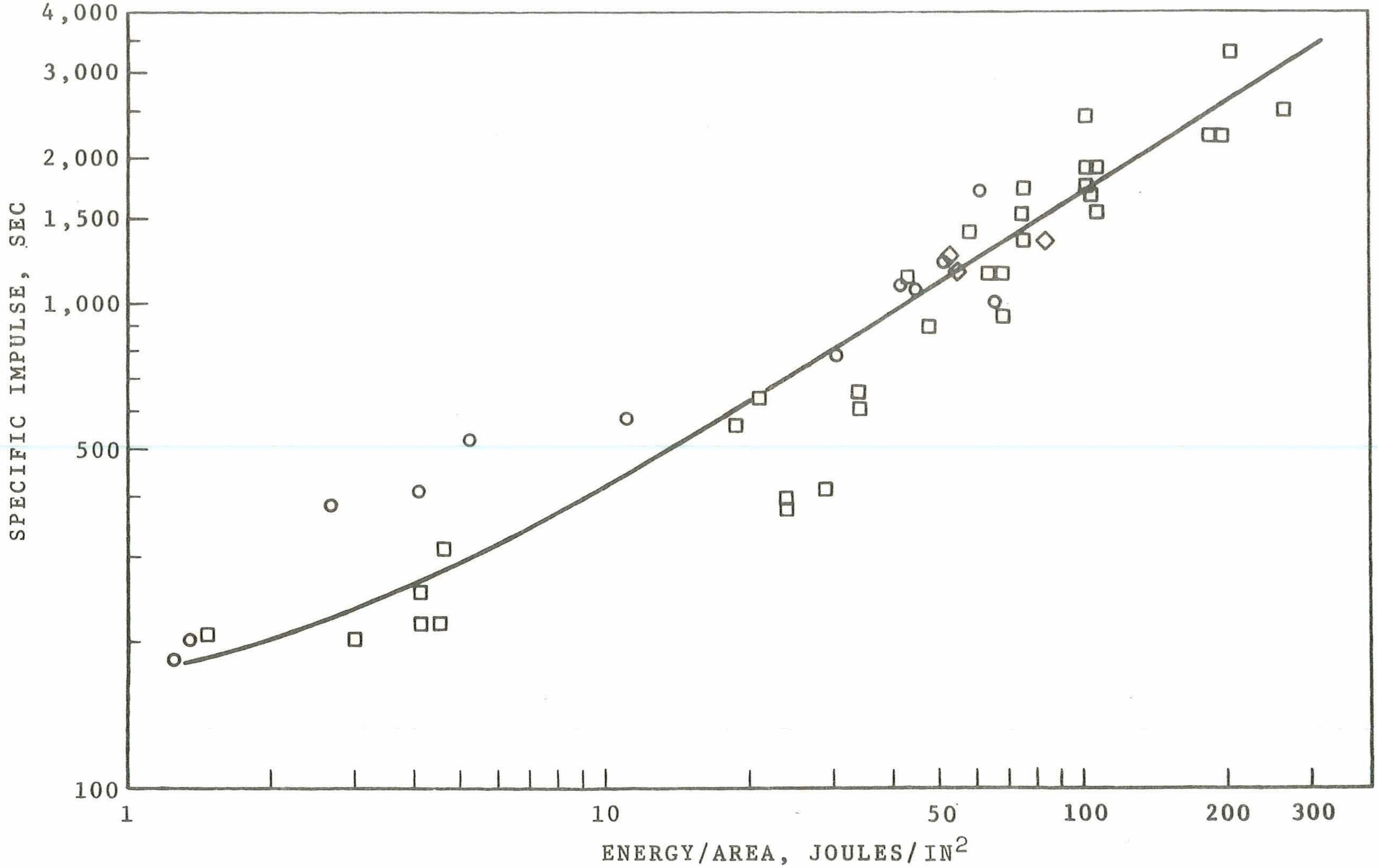

Figure 14. Specific Impulse as a Function of Discharge Energy Per Unit Propellant Area

thrusters. Also included are V-shaped propellants and the breech-plus-side-feed configuration (see Figure 7). A reasonably good correlation of specific impulse with the parameter energy per unit propellant area is found to exist for a wide variety of thruster configurations.

3.2.3.3 Discharge Energy/Propellant Mass Ratio

Simple idealized calculations[4] of thrusting mechanisms in the short pulse discharge thruster show thrust efficiency to depend upon the ratio of discharge energy to propellant mass per discharge. Figure 15 presents thrust efficiency as a function of this ratio. This discharge energy is the energy stored in the capacitor ($1/2CV^2$) uncorrected for losses and the mass is the total stored propellant mass change per discharge with no correction for mass utilization efficiency. The data of breech-fed thrusters is obtained from tests on a large number of thrusters with thrust levels varying from a few micropounds up to a few millipounds, and at discharge energies ranging from a few joules to a few hundred joules. The data of breech-fed thrusters presented shows a good correlation between the thrust efficiency and the energy/mass ratio. The two data points for breech-plus-side-feed (see Figure 7) shows efficiency significantly higher than breech-fed thrusters for the same value of the energy/mass ratio. It appears that more of the initial energy is transferred into kinetic energy of the mass aceelerated when propellant is also fed from the sides. Feeding propellant into the discharge from the downsteam side walls of the accelerator nozzle appears to provide sufficiently improved performance compared to a breech-fed thruster to consider side-fed thrusters as a separate class from breech-fed thrusters.

3.2.3.4 Electric Discharge Behavior

The earliest tests performed with the short pulse discharge thruster in the program were performed at an initial capacitor voltage of 1.1 KV. The discharge current was observed to be essentially critically damped. As capacitance and voltages were subsequently changed it was found that the discharge current became underdamped. The current reversals encountered, indicate that the interelectrode spacing designed for the low voltage (high capacitance) capacitor bank becomes mismatched when a high voltage-low capacitance capacitor bank is used. Since capacitor life is adversely

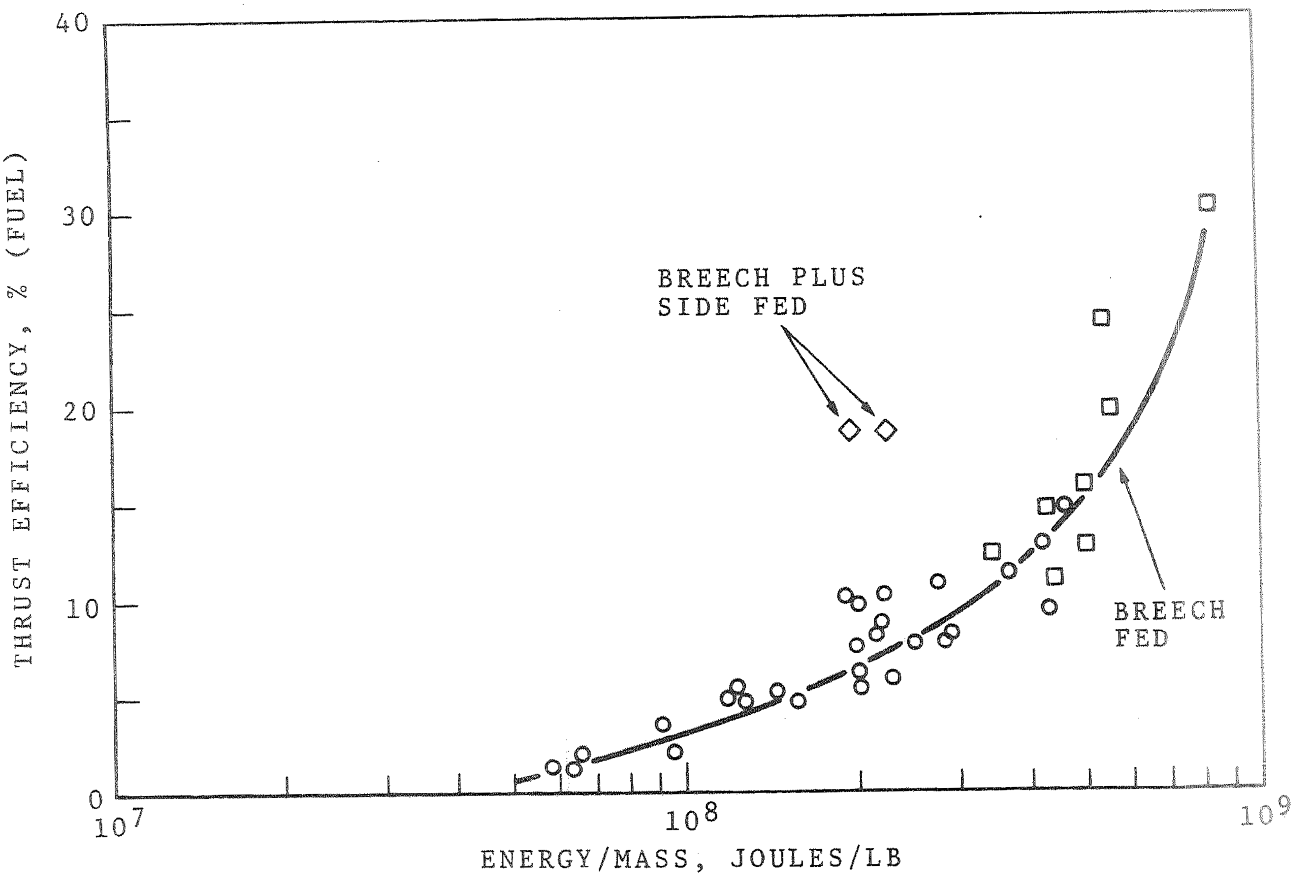

Figure 15. Thrust Efficiency as a Function of Energy/Mass Ratio (Short Pulse Discharge Thruster)

affected by such reversals oscilloscope pictures were examined in an attempt to qualitatively establish conditions for which a critically damped discharge will be observed. Figures 16a and 16b qualitatively present the general trend of the type of discharge as a function of parameters interelectrode spacing and voltage, initial field stress and capacitance, respectively. The results reveal changes to be made to convert a thruster having an oscillatory discharge to one which is critically damped.

a. For fixed capacitance, fixed gap: decrease voltage
b. For fixed capacitance, fixed voltage: increase interelectrode spacing
c. For fixed capacitance: decrease field strength (voltage/gap spacing)
d. For fixed field strength: decrease capacitance.

While oscillatory discharges are known to adversely affect capacitor life the slightly oscillating discharge (less than a 43% current reversal) encountered during the 3KV tests did not appear to adversely affect thruster performance.

3.2.4 Performance Extrapolation

An inspection of the performance data presented in Figure 8 shows that peak performance capability has evidently not yet been reached. This observation is made since the trend line of the data still shows no departure from a straight line variation. The straight line variation cannot extend indefinitely since it would eventually reach and exceed 100% efficiency. Starting at some value of specific impulse not yet reached, the data will eventually depart from the straight line. With the available data it is possible to determine the level of performance and the conditions that provide such performance that may be expected upon further development.

Figure 17 presents the product (impulse bit amplitude) x (specific impulse) as a function of discharge energy for a large number of short pulse discharge thrusters that have been experimentally evaluated during the present and previous microthruster programs. Several lines of constant efficiency are also shown. It is interesting to note that the experimental data obtained to date is roughly described by a straight line over approximately 4 decimal orders of magnitude of the parameter $(I_{sp}) \times (I)$. It is important to observe that the slope of this latter trend line is inclined relative to constant efficiency lines. While a range of efficiency can exist at a given discharge

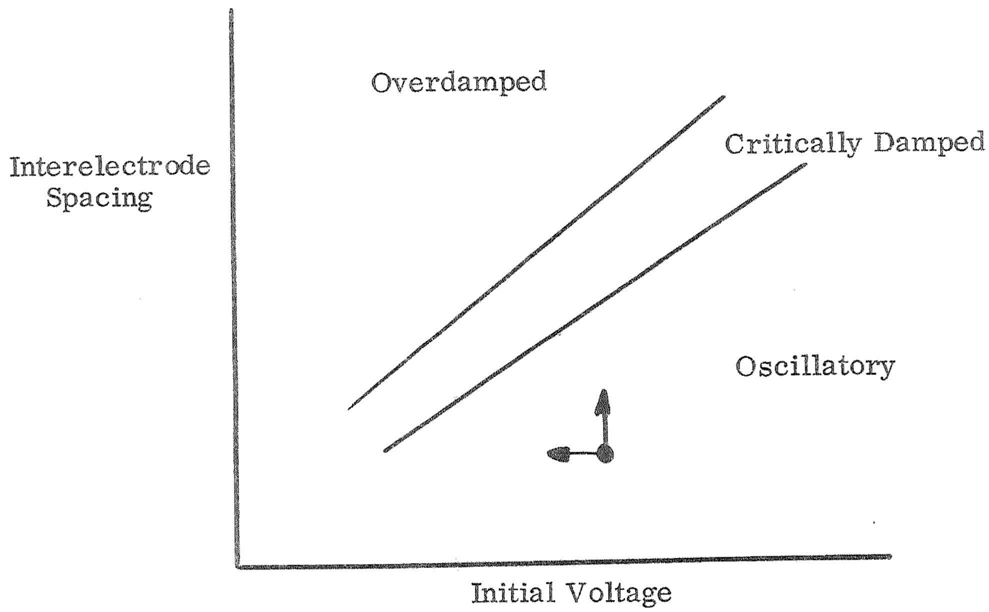

Figure 16a. Discharge Type as a Function of Spacing and Voltage

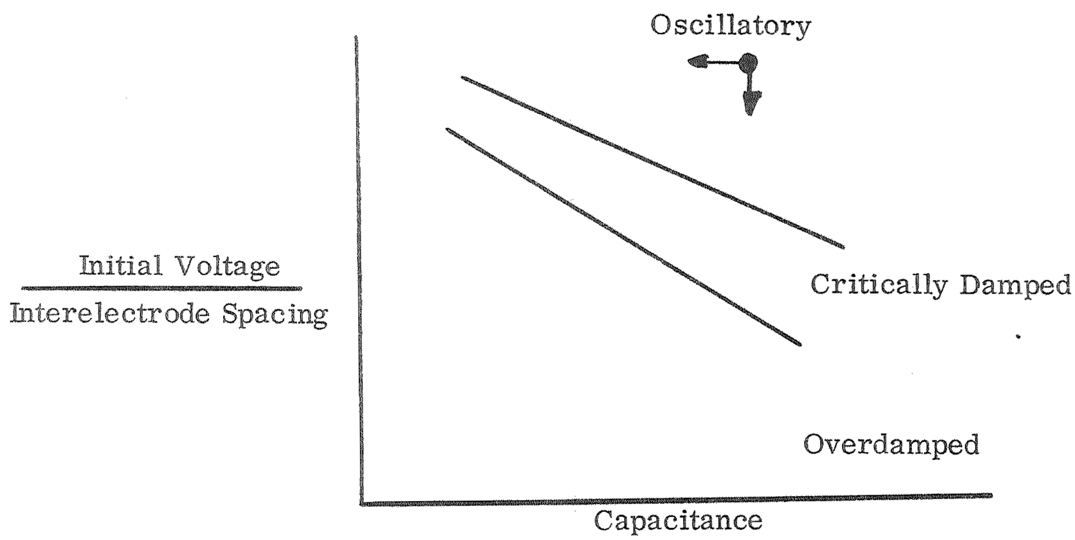

Figure 16b. Discharge Type as a Function of Initial Field Strength and Capacitance

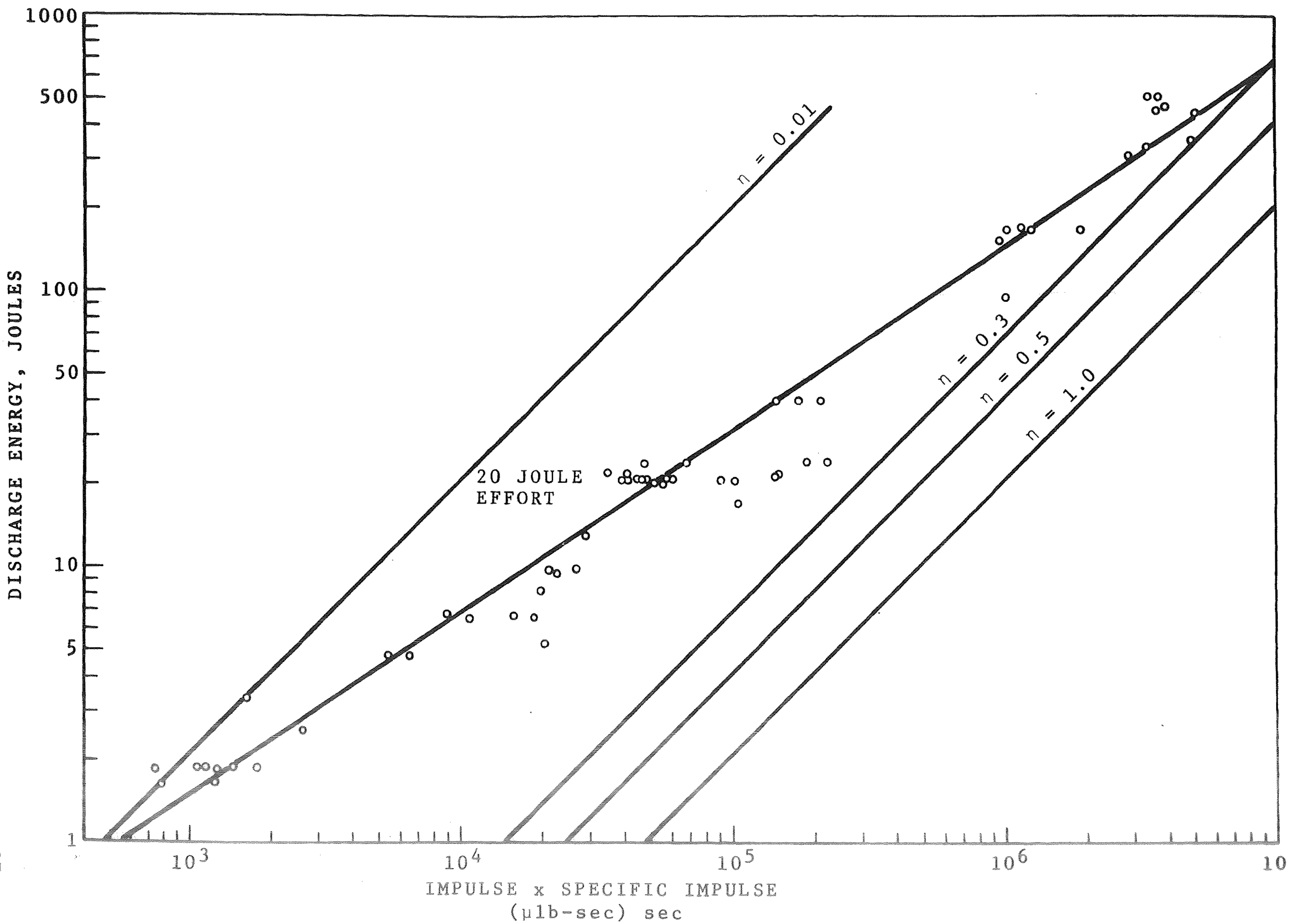

Figure 17. Discharge Energy as a Function of Impulse Bit x Specific Impulse

energy, the efficiency is seen to generally increase with an increase in discharge energy. If one extends the trend line of experimental data points to the intersection of appropriate efficiency lines, one finds approximately that:

η = 0.5 at a discharge energy of 1700 joules with $I\,I_{sp}$ = 40,000,000 μ lb-sec^2
η = 0.4 at a discharge energy of 1100 joules with $I\,I_{sp}$ = 21,000,000 μ lb-sec^2
η = 0.3 at a discharge energy of 600 joules with $I\,I_{sp}$ = 8,500,000 μ lb-sec^2

Since a number of data points exist to the right of the trend line, it is anticipated that it should be possible to reach the latter efficiencies at lower discharge energies than the general trend line predicts. The above extrapolations are interesting since they enable predictions to be made of the performance to be expected at energy levels not yet examined in this country. One Russian reference[12] has already examined certain aspects of teflon propellant accelerators up to 4950 joules. However, no propulsion data was reported in Reference 12 or any other Russian references.[13,14]

From the above extrapolated data one finds the specific impulse to be given by the values presented in Table 7. While in the present program a performance level has already been experimentally reached by a few research thrusters compatible with stationkeeping requirements of either 3-axes or spin stabilized satellites, the extrapolated performance of Table 5 reveals that substantial improvements over present results may be expected at higher discharge energy levels than those used in the present study.

TABLE 7. Extrapolated Performance

η (%)	$I\,I_{sp}$ (μ-lb-sec^2)	E (joules)	P/T	156.5	125	100 watts/milli-lb
			T/P	6.39	8.0	10.0μ lb/watt
0.3	8,500,000	600		2220	1770	1415
0.4	21,000,000	1100		2980	2390	1910
0.5	40,000,000	1700		3680	2940	2350

SECTION 4

QUASI-STEADY THRUSTER

4.1 DESIGN

The comparison between solid propellant quasi-steady thruster operation and solid propellant short pulse discharge thruster operation was to be made under similar as possible conditions. As design inputs, it was therefore assumed that: (1) the electrode nozzle and solid propellant geometry of either configuration being compared would be the same, and (2) the magnitude of the dynamic impedance of the plasma during the acceleration phase of the short pulse discharge thruster (see Section 3.2.2.1) could be used as the load impedance in the design of the pulse forming network (PFN) for the quasi-steady thruster.

Due to the low dynamic impedance of 6.5 milliohms either of two approaches could be followed in the design of the PFN. In one case a pulse transformer could be utilized to achieve a good impedance match between the discharge circuit and the plasma, in the second case no transformer would be used but a bank of capacitors having a large capacitance. The latter approach was selected for economic reasons. In order to be able to accommodate the weight of the bank of capacitors on the available thrust balance it was necessary to use electrolytic capacitors. Since electrolytic capacitors had been previously used for such purposes[7,8] no outstanding problems in the design and use of such a network was expected.

Besides the above considerations it was desirable to have a peak power of the order of 10^6 watts during the quasi-steady acceleration phase, a pulse length of at least 100μ sec and a discharge current of the order of 10Ka.

Since the PFN must be placed in a fairly compact package on the thrust balance it was decided to minimize the effects of mutual inductance in the PFN by using a Type C instead of a Type D (equal capacitance) network[15] conventionally used.

Figure 18 shows a schematic of this idealized 5-section circuit used:

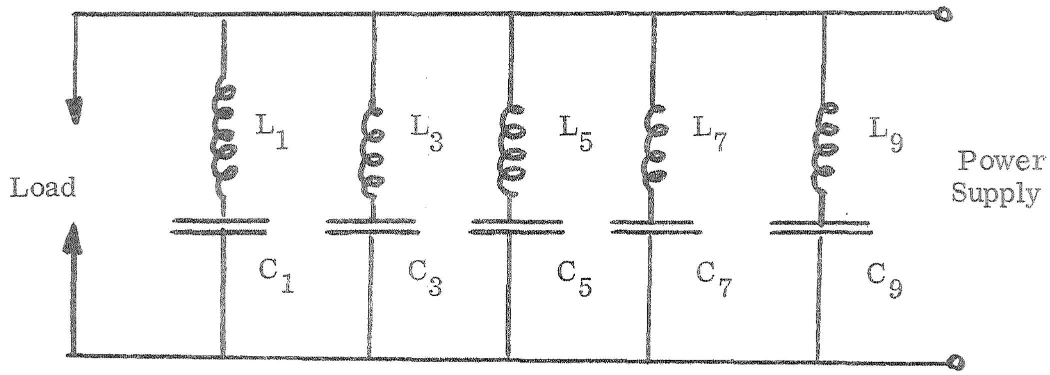

Figure 18. Schematic of 5-Section Circuit

The numerical values for inductance and capacitance were calculated from the nondimensional values presented for an idealized network in Reference 15. For a pulse duration of 100μ sec with a parabolic rise and fall time of 5% one has the following nondimensional values of inductance and capacitance.

$L_1 = 0.2507$	$C_1 = 0.4042$
$L_3 = 0.2547$	$C_3 = 0.04420$
$L_5 = 0.2632$	$C_5 = 0.01539$
$L_7 = 0.2773$	$C_7 = 0.00745$
$L_9 = 0.2961$	$C_9 = 0.00422$

For a load impedance of 6.5 milliohm and a desired pulse duration of 100 μ sec one finds actual inductance and capacitance to be as follows:

$L_1 = 0.162 \times 10^{-6}$ Henries	$C_1 = 6212\ \mu$ fd
$L_3 = 0.165 \times 10^{-6}$ Henries	$C_3 = 679\ \mu$ fd
$L_5 = 0.171 \times 10^{-6}$ Henries	$C_5 = 236\ \mu$ fd
$L_7 = 0.180 \times 10^{-6}$ Henries	$C_7 = 114\ \mu$ fd
$L_9 = 0.192 \times 10^{-6}$ Henries	$C_9 = 69.9\ \mu$ fd

It is perhaps interesting to note that a Type D (equal capacitance) circuit would require 5 x 1398 or 6980 μfd. The total capacitance of the unequal section circuit will be 7310 μfd. While either circuit would weigh about the same, it was believed that the Type C circuit would be easier to assemble in a smaller package.

The above idealized considerations neglect the inductance due to the capacitors and the current collection assembly of the network. Since no control existed on the inductance of the electrolytic capacitors, the network was designed to have as low an inductance as possible. The above listed idealized coil inductances were then considered to include the inductance of capacitors. The 5 sections of the network were assembled of custom 450 volt Aluminum electrolytic capacitors provided by the Mallory Capacitor Company. A comparison between theoretical and actual capacitance for each of the five sections is as follows:

Section	Theoretical Cap.	Actual Cap.	C_{act}/C_{th}
1	6212 μfd	6380 μfd	1.027
2	679	644.4	0.949
3	236	213	0.902
4	114	104	0.912
5	69.9	83	1.187
Total	7310.9	7424.6	1.016

The theoretical circuit was reasonably well simulated with respect to capacitance. To minimize circuit inductance the capacitors of each section were first collected in parallel by a low inductance disk assembly. The current of each disk assembly was then transferred through a short low inductance coaxial section into a common low inductance strip line. The thruster electrode nozzles were fastened directly to one end of this strip line. Figure 1 shows the final thruster and PFN network.

Before the network was used for performance studies it was bench checked at low voltage (below 10 volts) for discharge current waveform. In order to facilitate bench testing the plasma load whose impedance was measured to be 6.5×10^{-3} ohm was simulated by a 4.45 cm long thin wire. The inductive impedance $X_L = 2\pi f L_{wire}$ was calculated and found to be roughly two orders of magnitude lower than its resistance*. Initial bench tests revealed that the inductance of the Mallory electrolytic capacitors was sufficiently high such that the original design values of the inductors had to be modified. After readjusting the circuit parameters (L and C) an acceptable square wave was obtained (see Figure 19) at low voltage. The long exponential decay and reversals are undesirable but could not be improved upon with the capacitors in the circuit. The final capacitance was 7134.6 μfd and the pulse duration of constant current at low voltage is about 83μ sec.

Prior to the installation of the quasi-steady thruster on the thrust balance, a thermocouple was attached to each capacitor of the network. The output of each thermocouple was fed into a thermocouple switch whose output is fed directly into a Honeywell Model 906C Visicorder with a M-100-120A galvonometer. This setup readily enables the temperature variation of all capacitors to be quickly monitored and recorded during thruster operation. As suspected, one capacitor was found to heat up faster than the remaining ones. Duration of thruster operation is limited by the temperature of this one capacitor. Operation was stopped whenever the temperature of this one capacitor reached about 110-130°F. The subsequent temperature rise still keeps the peak temperature below 140°F.

----

* Measured by Kelvin Bridge Ohmmeter No. 4285 Leeds & Northrup Co. range 0.0001 ohms to 26.6 ohms

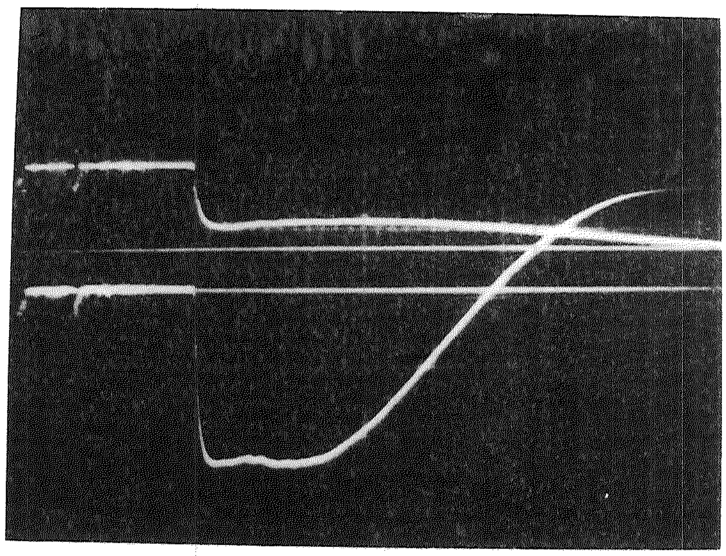

Figure 19. Square Wave of Pulse Forming Network
(Low Voltage Bench Test)
50 μ sec/cm

Acceptable operation without localized arcing could only be accomplished by sealing the anode to the strip line. Unfortunately this solution made it impossible to measure anode erosion. Cathode and insulator erosion and propellant consumption were measured in the same manner as with the short pulse discharge thruster.

4.2 EXPERIMENTAL RESULTS

Initial full voltage thruster tests with the quasi-steady thruster showed a strong current overshoot on the initial sharp current rise. Since attempts to eliminate the overshoot affected the duration of the constant current region, performance data was taken with the current overshoot. Figure 20 shows a typical discharge voltage and current trace at the same sweep speed as the low voltage test (Figure 19). In comparing the thruster data with the low voltage bench test data (Figure 19), it is noted that a roughly 50% current reversal occurred in both cases.

Voltage

Current

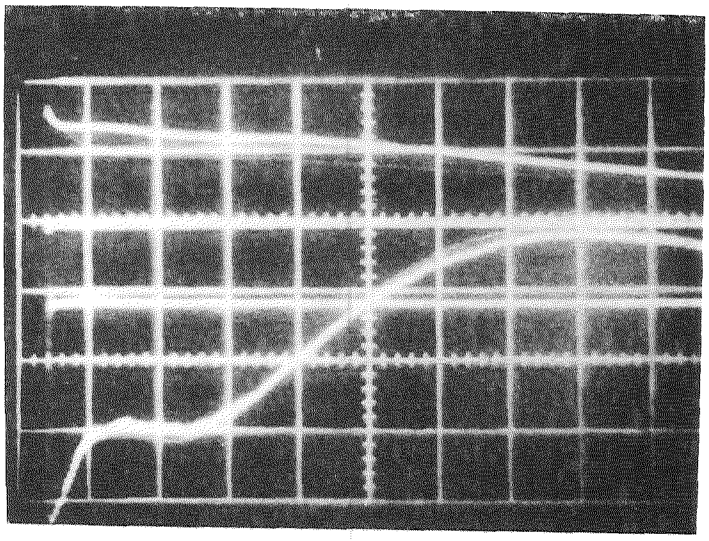

Figure 20. Typical Discharge Voltage and Current Trace during Quasi-Steady Thruster Operation 50μ sec/cm (n=906)

The duration of the steady current is roughly 80 μ sec in both cases as well as a duration of positive current for about 220 μ sec. The essential difference between both cases is the presence of the strong initial current overshoot observed during quasi-steady thruster operation. Figure 21 shows another typical discharge voltage and current trace at a sweep speed of 20 μ sec/cm. Both the voltage and current are seen to be relatively free of noise. Malliaris[7] finds that quiet voltage traces such as those presented in Figures 20 and 21 are for conditions which he refers to as being below critical, i.e., not too severe an erosion. Data to be presented in Section 4.3.2 will show that even though according to the voltage criteria relatively low erosion is expected, the erosion measured was substantially larger than encountered during short pulse operation.

Voltage

Current

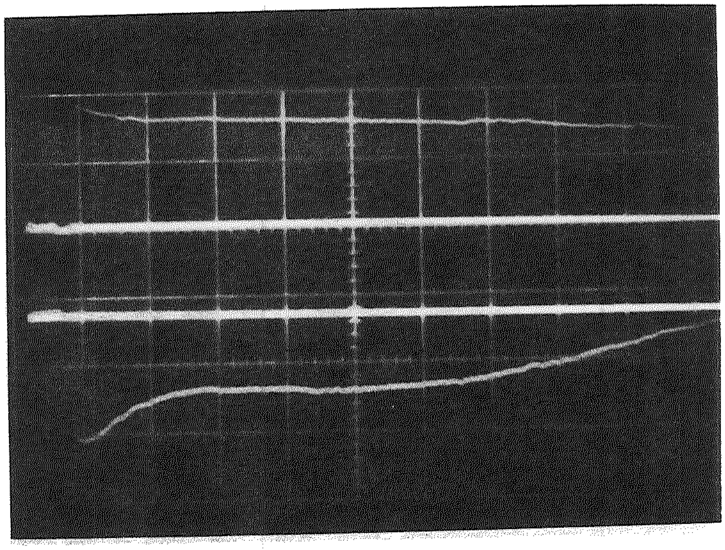

Figure 21. Typical Discharge Voltage and Current Trace during Quasi-steady Thruster Operation (20 μ sec/cm)

4.2.1 Performance

Performance data of the quasi-steady thruster was taken in the same manner as for the short pulse thruster. Four sets of experiments were performed. The data of these four tests are presented in Table 8, in the same format as the results for the short pulse thruster studies (see Table 2). During all four tests performed with the quasi-steady thruster unsatisfactory depolymerization of the teflon propellant was observed. An examination of the propellant after operation showed that the face of the teflon had black regions of teflon. Figure 22. shows the propellant, cathode and insulator assembly after breech fed tests 128x-1 and 128x-2 and breech plus side feed tests 128x-3 respectively. The propellant face after test log 128x-1 was found to be darker than that encountered with 128-x-2. Prior experience at Republic with short pulse dischsarge thrusters show that a darkened propellant face provides performance corresponding to a higher than normal specific impulse and a lower than normal

TABLE 8. Quasi-Steady Thruster Data

	Breech		Breech-plus-side-feed	
Capacitor energy in joules	321<E<376	484.5	529.2	349
Propellant area, in^2	1.69	1.69	5.51	5.51
Capacitance, μfd	7134.6	7134.6	7134.6	7134.6
Initial voltage, V	301<V<325	369	385	313
Shots of Test	5730	1970	1636	1502
Pulse frequency, Hz	0.560	0.581	0.67	0.696
Test duration at f, Hrs	2.84	0.945	0.678	0.600
Test avg thrst, μ lb	264	758	1211.8	616
Impulse bit, I, μ lb-sec	472	1306.8	1809.1	884
Propellant spec. Imp., sec	3070	2680	1340	975
Thrust eff. $\eta(E_s, m_p)$, %	8.4< η < 9.85	15.75	10.0	5.38
Thrst/pwr ratio, (I, E_s) mlb/kw	1.25<I/E< 1.47	2.70	3.42	2.53
Pwr/thst ratio, (E_s, I) w/mlb	6.80<P/T< 800	370	292	396
Delivered engy, joules	185.3	339.5	327.4	228
Engy trnsf eff (E_d/E_s), %	49.2< η <57.8	70	61.7	65.4
Total mass spec. imp., sec	---	1970	1265	925
Thrst eff, $\eta(E_d, m_p)$, %	17	22.5	16.1	8.24
Thrst eff. $\eta(E_s, m_t)$, %	---	11.58	9.45	5.1
Thrst eff. $\eta(E_d, m_t)$, %	---	16.5	15.2	7.81
i^2/m	34	21	6.5	8.6
Log #	128x1	128x2	128x3	128x4

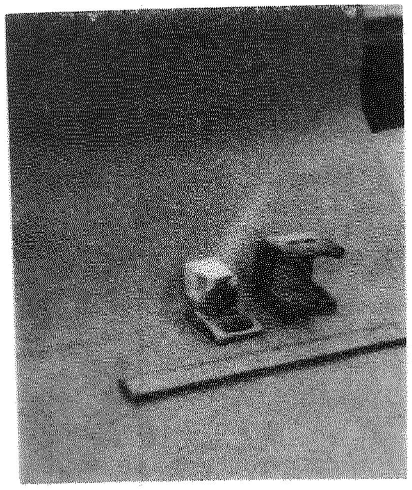

a) Log 128x-1

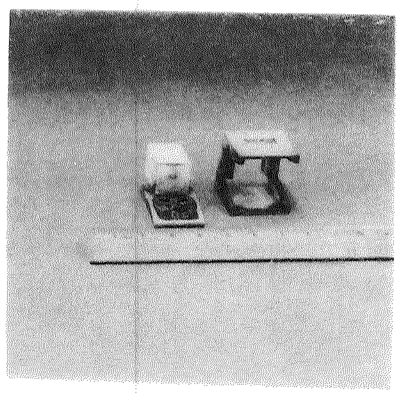

b) Log 128x-2

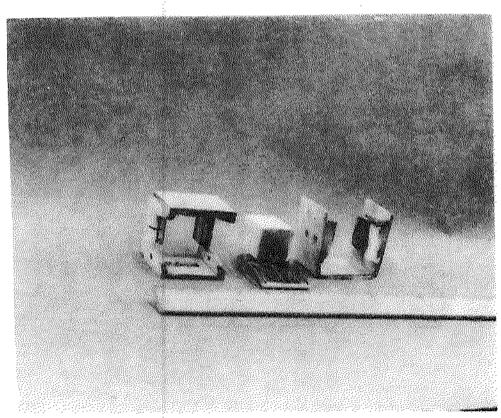

c) Log 128x-3

Figure 22. Propellant, Cathode, and Insulator Assembly after Quasi-Steady Thruster Operation

thrust/power ratio. Generally such a condition is eliminated by operating the given thruster at a higher initial voltage in order to increase the discharge energy.

The performance of the first set of data, Log 128x-1 in comparison to the remaining three sets of data does not have the same general trend as the latter data when propellant specific impulse is presented as a function of efficiency $\eta\ (E_s, m_p)$. A comparison of the discharge current and voltage traces of the four tests show that the discharge current for test 128x-1 was occasionally "noisy" during the test. Figure 23 presents one typical "noisy" discharge current trace observed during test 128x-1.

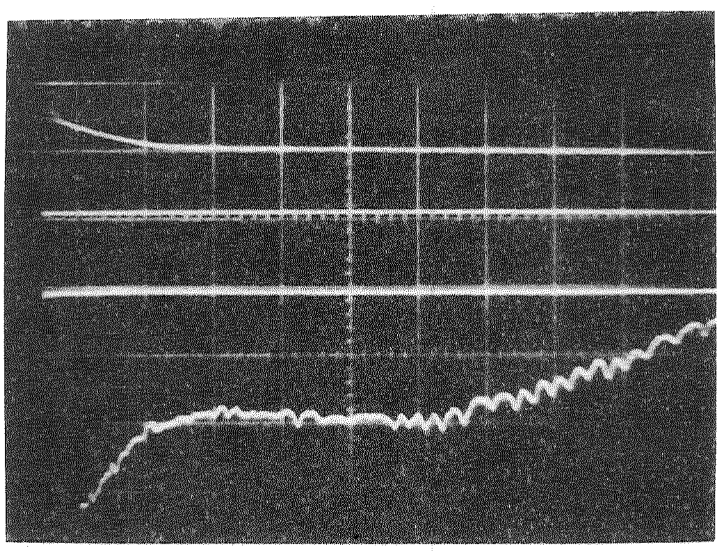

Voltage

Current

Figure 23. "Noisy" Discharge Current Trace During Test 128x-1
(20μ sec/cm)

This latter trace can be compared to the "quiet" type of discharge current observed during all three of the other quasi-steady thruster tests performed. Interestingly Malliaris observes the discharge voltage to be noisy when his quasi-steady thruster is operating in the propellant underfed condition. This latter condition is marked by a high erosion rate. The terminal discharge voltage of test 128x-1 shown in Figure 23 is seen to be as free from spikes as the voltage traces of the other three quasi-steady thruster tests (see Figure 22 for example).

While values of impulse bit amplitude and either propellant specific impulse or total mass specific impulse have been measured in a regime of interest to propulsion, the relative merit of the values is more meaningful when compared with short pulse discharge operation. Such a comparison is presented and discussed in Section 5.1.

4.2.2 Erosion

Erosion studies were made of the cathode and insulator assembly for the last three tests. As mentioned earlier, anode erosion could not be measured since satisfactory operation of the quasi-steady thruster was only possible when the anode was sealed to the strip line assembly.

Table 3b presents the quasi-steady thruster erosion data in the same format as the short pulse erosion data. Since anode erosion could not be measured it is not possible to quantitatively assess relative erosion between the anode, cathode and insulator. Visually, the anode appeared to experience a greater erosion than the cathode. Essentially all of the anode erosion took place at the two downstream corners of the anode. The erosion results are more meaningful when compared with the results obtained during short pulse thruster operation. Such a comparison is presented in Section 5.2.

SECTION 5

PERFORMANCE COMPARISON

5.1 PROPULSIVE PERFORMANCE

In Section 2 it was shown that propulsive performance can be calculated in any one of a number of ways. When making comparisons between short pulse discharge and quasi-steady thruster performance such differences must be considered. From propulsive system considerations the thrust efficiency $\eta(E_s, m_p)$ and propellant specific impulse are important parameters. Figure 24 presents thrust efficiency as a function of propellant specific impulse for both breech-plus-side-fed and breech fed thruster operation of short pulse discharge and quasi-steady thrusters. Compared in this manner, the breech-plus-side-fed short pulse discharge configuration provides a significantly better level of performance than either the breech fed short pulse or either of the quasi-steady thruster configurations. For example, at a given specific impulse the efficiency of the short pulse breech-plus-side-fed configuration is twice that of either type of quasi-steady thruster configuration and about 50% higher than the short pulse breech fed configuration.

In making the above comparison, it must be remembered that tests were performed with the same accelerator nozzles. It is quite possible that nozzle geometry requirements for optimum performance of a quasi-steady thruster differ from those of a short pulse discharge thruster. Such considerations were beyond the scope of the present study, however, such a possibility is not excluded since a visual inspection of the erosion pattern of the electrodes and side propellant suggests that the arc during most of the discharge of the short pulse thruster remains attached at the fuel retaining shoulder while for quasi-steady operation it is swept downstream and remains most of the time at the downstream extremities of the electrodes. (see Figure 22c for example).

The above comparison does not take into account that the electrolytic capacitors in the pulse forming network of the quasi-steady thruster dissipate more energy than the energy storage capacitors of the short pulse discharge thruster circuit.

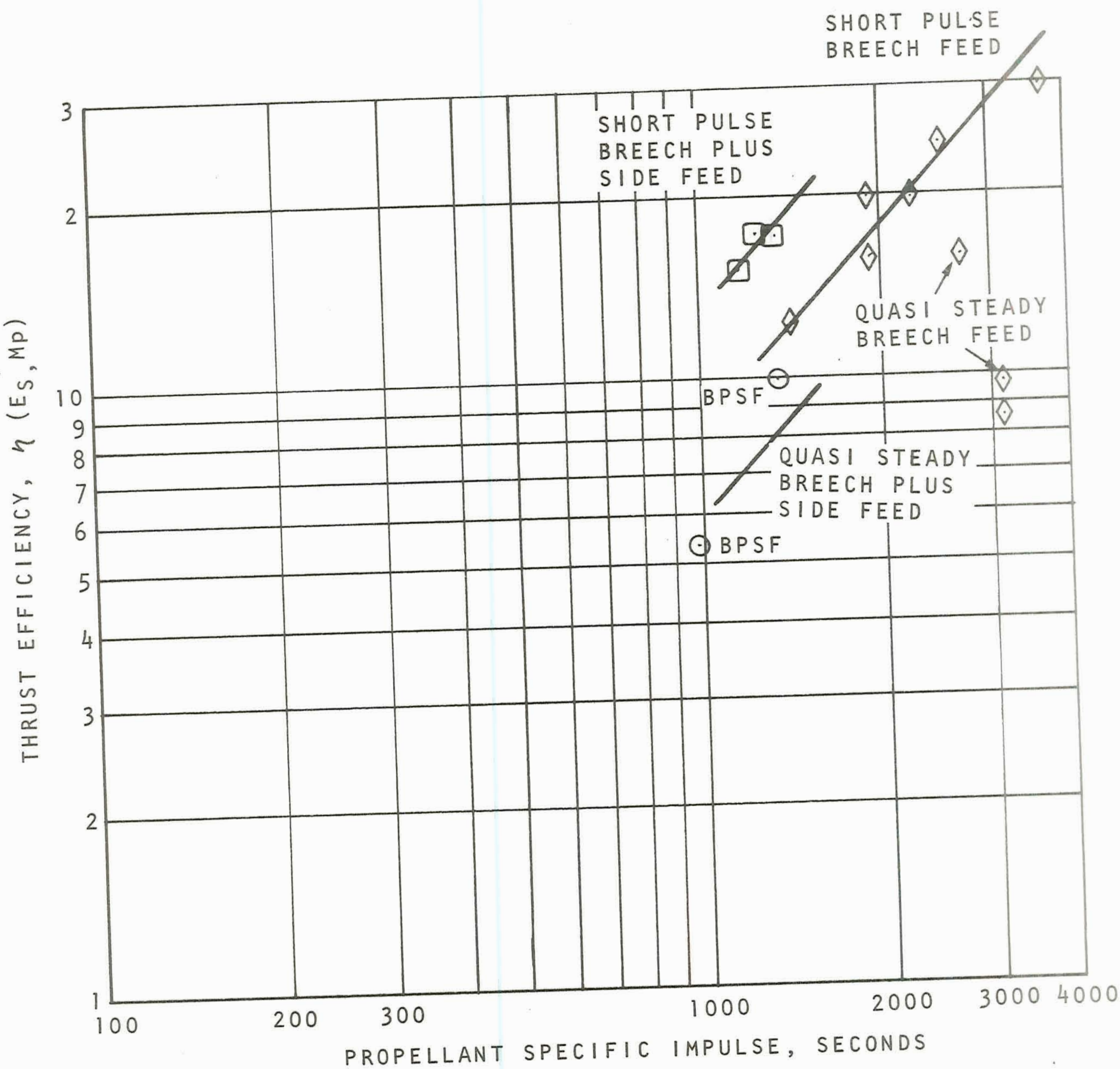

Figure 24. Performance Comparison $\eta(E_s, m_p)$ Versus I_{sp}

Presenting efficiency $\eta(E_d, m_p)$ as a function of propellant specific impulse compares performance using only the quantity of electric energy delivered into the accelerator nozzle. Figure 25 presents such a comparison of the performance of short pulse discharge thruster and quasi-steady thruster. Because of the relatively few data points and the differences in performance noted between breech fed and breech-plus-side-fed configurations some caution must be exercised in drawing general conclusions. Based upon the available data, it is seen that again the short pulse breech-plus-side-fed configuration has a somewhat better performance than any of the other configurations tested. With the exception of one quasi-steady data point (Log 128x-1) the data points of either short pulse breech fed or the quasi-steady configurations tested are very nearly described by a single trend line. With the exception of the short pulse breech-plus-side-fed configuration there does not appear to be any marked superiority in performance of any one of the three other configurations when compared on the basis of delivered energy and propellant specific impulse.

5.2 EROSION

Table 3 summarizes erosion data obtained during diagnostic tests of the short pulse discharge and quasi-steady thrusters. Since anode erosion could not be measured for the quasi-steady thruster, a direct comparison of erosion can only be made for the sum of cathode plus insulator erosion. In Section 3.2.2 it was pointed out that erosion may be examined either as percent of propellant mass consumed or eroded mass per total impulse delivered. Figure 26 presents percent cathode plus insulator erosion as a function of propellant specific impulse. Compared in this manner, it is seen that erosion (%) during quasi-steady thruster operation is significantly larger than that encountered during short pulse discharge operation. Figure 27 presents erosion (cathode plus insulator) as pounds of eroded cathode plus insulator per pound-second of total impulse delivered. In this comparison it is again seen that erosion (lb/lb-sec) during quasi-steady operation is about an order of magnitude larger than short pulse discharge operation.

The data presented in Figures 26 and 27 show that cathode plus insulator erosion expressed either as percent of propellant mass used, or as pounds per pound-second total impulse delivered is significantly lower during short pulse discharge thruster operation. While anode weight measurements could not be made on the quasi-steady thruster, strong erosion of the anode was always observed. It is believed that

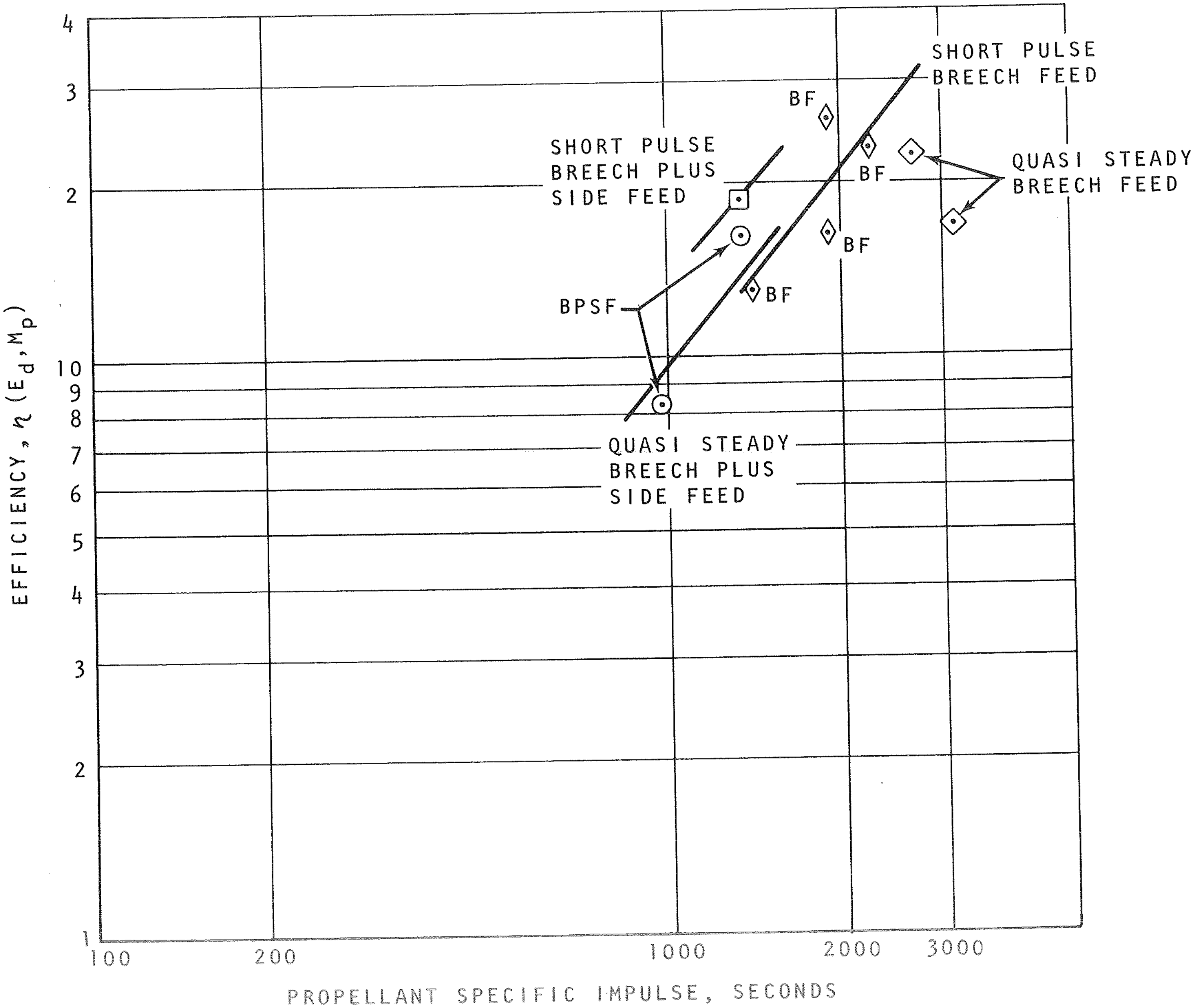

Figure 25. Performance Comparison η (E_d, m_p) Versus I_{sp}

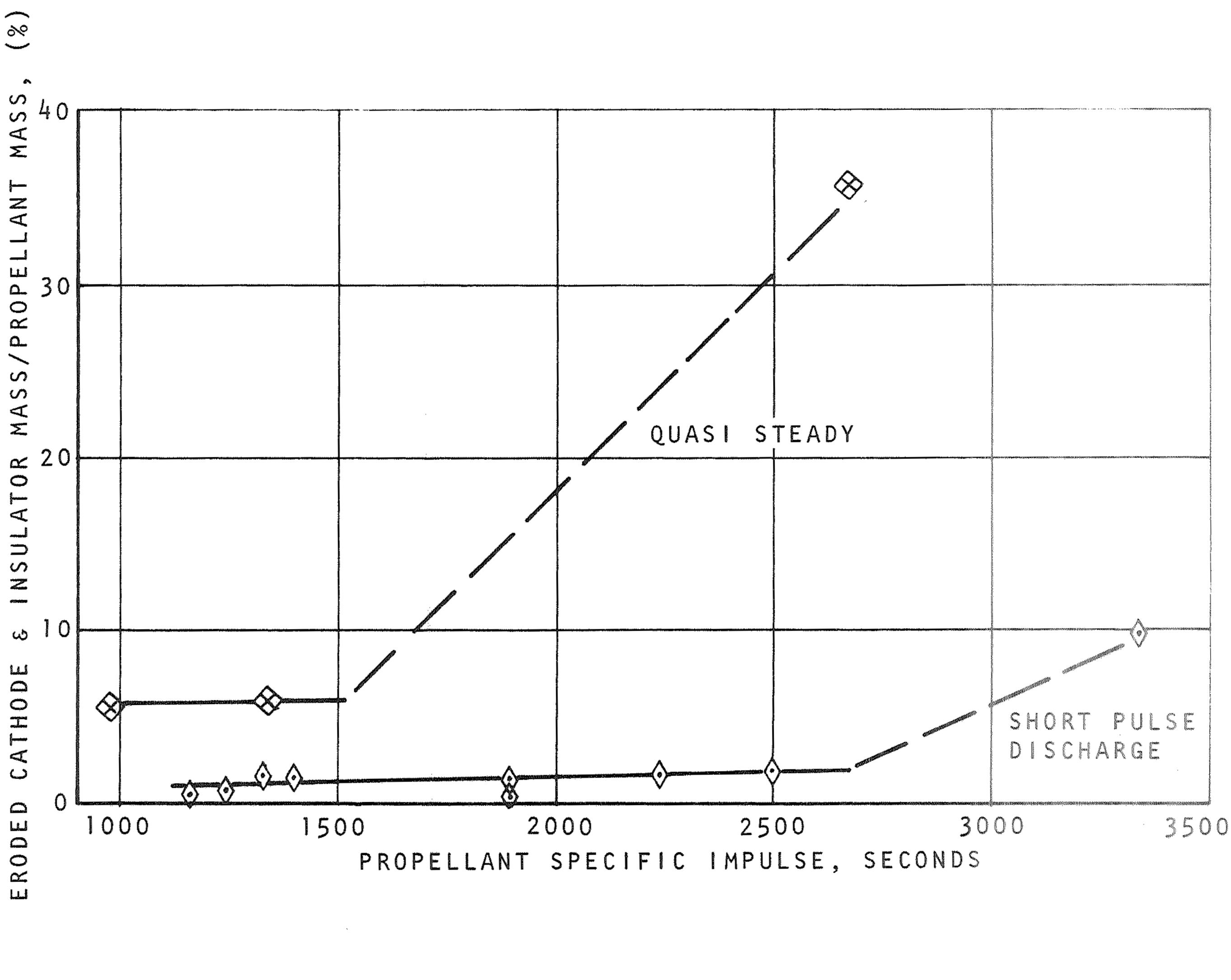

Figure 26. Percent Cathode plus Insulator Erosion as a Function of Propellant Specific Impulse

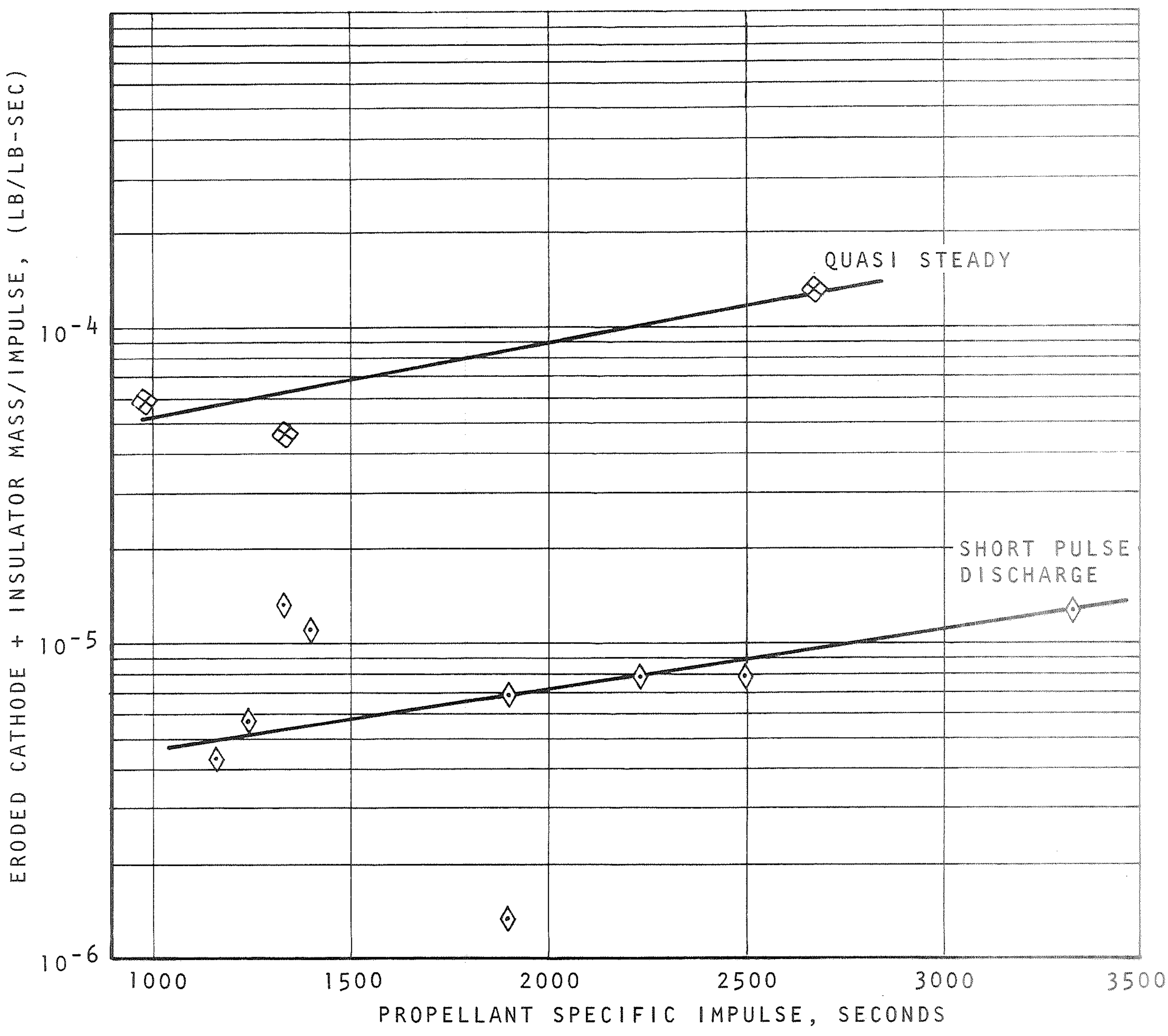

Figure 27. Erosion (Cathode plus Insulator) Expressed as lb per lb-sec. Total Impulse as a Function of Specific Impulse

even if anode weight measurements could have been made that total erosion (anode plus cathode plus insulator) would have been lower on the short pulse discharge thruster. It should be remembered that the same electrodes were used for the tests. As mentioned in Section 5.1, it cannot be ruled out that an electrode geometry appropriate for short pulse operation may be undersirable for quasi-steady operation. Such electrode geometry considerations were beyond the scope of the present effort.

SECTION 6

CONCLUSIONS

Conclusions drawn on the basis of the work performed are briefly summarized below. Details of the results upon which these conclusions are based are presented in the main body of this report.

A. Results have shown that providing propellant from the downstream sides of the discharge in addition to that provided from the breech end significantly improves the thrust/power ratio and substantially reduces erosion compared to normal breech fed thrusters. Furthermore, since the performance data of such configurations does not correlate with breech fed thruster data, the technique is considered to provide a new class of thruster having substantially better performance than breech fed thrusters.

B. The breech fed teflon propellant short pulse discharge microthruster can be scaled predictably from the micro-pound thrust level regime to the millipound thrust regime using the correlation of I_{sp} with E/A. In the millipound thrust regime the measured performance of η with I_{sp} and I I_{sp} with E_d, respectively, was found to be in the general range of interest to North-South stationkeeping of satellites.

C. Even though a thrust efficiency of 30% was realized, optimum propulsive performance has not yet been achieved with the short pulse discharge thruster. Substantially higher efficiency is expected by increasing the discharge energy to values several times larger than those examined in this study.

D. Expressing erosion as percent of propellant consumption is found to vary linearly with specific impulse. Such a correlation can erroneously suggest prohibitive erosion when the thruster operates at higher levels of specific impulse. The proposed erosion parameter which expresses the ratio of the quantity of eroded mass to the total impulse delivered is believed meaningful for practical applications. This latter erosion parameter was also found to increase with specific impulse bit at a rate which does not suggest prohibitive erosion when a thruster is operated at a higher specific impulse to deliver a given value of total impulse.

E. Results show electrode material and the duration of a test to affect either of the two erosion parameters cited in this study. Since the scope of the effort was limited with regard to the number of different material evaluations further experimental studies should be carried out to comprehensively compare material quantitatively before any final conclusions are made on the level of erosion expected in practical applications.

F. While the present results show solid propellant short pulse discharge thruster operation to provide a better performance at a lower erosion level than solid propellant quasi-steady operation when compared under similar conditions, it is important not to consider the present results conclusively proving that short pulse operation is generally superior to quasi-steady operation. The scope and duration of the program limited the number and range of data points obtained. It is hoped the present results will suggest future studies of a similar nature to provide more data over a wider range of operating parameters.

SECTION 7

REFERENCES

1. Guman, W. J., Nathanson, D. M., Pulsed Plasma Microthruster Propulsion System for Synchronous Orbit Satellite, J. Spacecraft & Rocket, Vol. 7, No. 4, April 1970, pp 409.

2. Pearson, J., Loddengaard, R., An Impulse Balance System, PCD-TR-64-10, RAC 2388, Republic Aviation, June 1964.

3. Guman, W., Truglio, W., Surface Effects in a Pulsed Plasma Accelerator, AIAA Journal, July 1964, pp 1343.

4. Guman, W., Pulsed Plasma Technology in Microthrusters, AFAPL-TR-68-132, Air Force Aero Propulsion Laboratory, Dayton, Ohio, November 1968.

5. Vondra, R., Personal Communication, MIT Lincoln Lab (1971)

6. Vargo, D. J., Taylor, F. L., Electrode Erosion in Spark Discharges, J. Appl. Physics, Vol. 33, No. 9, pp 2911/12, September 1962.

7. Malliaris, A. C., Jahn, R. R., Garrison, R. L., Libby, D. R., Quasi-Steady MPD Propulsion at High Power, NASA CR 111872, Final Technical Report, AVSD-0146-71-RR, Avco Corp., Wilmington, Mass., Feb. 1971.

8. Ducati, A. C., Jahn, R. G., Exploratory Electromagnetic Thruster Research, NASA CR 66923, Report FR-020-9297, Plasmadyne, Santa Ana, Calif., Feb. 1970.

9. Cobine, J. R., Gaseous Conductors, Dover Publications, NY, 1958, pp 177.

10. Michaels, C. J., Dynamic Current-Voltage Characteristics of a Nitrogen MPD Arc Plasma Source, NASA TMX-52681 (1969).

11. Andreev, S., Vanyukov, M., Application of a Spark Discharge to Obtain Intense Light Flashes of Length $10^{-7} - 10^{-8}$ sec., Sov. Phys. - Tech. Phys. Vol. 6, No. 8, Feb. 1962, p. 700.

12. Balagurov, A., Grishin, S., Levtov, V., Leskov, L., Mikhalev, V., Petrov, A., Savin, A., Savichev, V., Chivilev, V., Characteristics of Plasma Acceleration in Electromagnetic Accelerators with Dielectric Erosion, Sov. Phys.-Tech. Phys. Vol. 15, No. 3, Sept. 1970, p. 345.

13. Kalygin, A., Kozlov, N., Leskov, L., Saenko, V., Current Distribution in Pulsed Plasma Accelerator with Dielectric Erosion, Sov. Phys.-Tech. Phys. Vol. 15, No. 3, Sept. 1970, p. 355.

14. Kalygin, A., Kozlov, N., Koreshchenko, N., Leskov, L., Saenko, V., Energy Characteristics of a Pulsed Dielectric Erosion Plasma Accelerator, Sov. Phys. -Tech. Phys. Vol. 15, No. 6, Dec. 1970, p. 928.

15. Glasoe, G.N., Lebccgz, J.V., Pulse Generators, McGraw Hill Book Co., 1948, New York, p. 202.

16. Fricke, R.H., Garber, T.B., Perturbation of a Synchronous Satellite, R-399-NASA, The Rand Corp., May, 1962.

17. Shattuck, R., Sohl, G., Toms, R.S.H., Electric Propulsion for Satellite Position and Attitude Control, AIAA paper 67-722, Sept., 1967.

APPENDIX A

NORTH-SOUTH STATIONKEEPING CALCULATIONS WITH A PULSED PLASMA PROPULSION SYSTEM

The simplified analysis presented below were performed in an attempt to assess pulsed plasma propulsion system performance requirements to perform North-South stationkeeping of synchronous satellites:

Let	I	=	total impulse (lb-sec)
	i	=	total impulse per thruster
	i_n	=	total impulse at each nodal pass per thruster
	i_b	=	impulse bit amplitude per thruster
	A	=	mission time of I (in years)
	W	=	weight of spacecraft (lb)
	g	=	gravitational constant (32.2 ft/sec^2)
	ΔV	=	velocity increment ft/sec/year
	R	=	weight of propellant required (lb)
	θ	=	degrees of firing about a nodal point to delivery required total impulse
	T	=	thrust level (lb)
	P	=	power (kw)
	τ	=	duration of thruster firing about a node (hrs)
	I_{sp}	=	specific impulse (sec)

The total impulse required for a mission time of A years is:

$$I = A \frac{W}{g} \Delta V \tag{1}$$

PART 1, 3-AXES STABILIZED SATELLITE WITH N/S THRUSTER PAIR

For this case each thruster must provide I/2 lb-sec of impulse

$$i = I/2 = \frac{A}{2} \frac{W}{g} \Delta V \tag{2}$$

The quantity (R) of propellant required is thus:

$$R = i/I_{sp} = \frac{A}{2} \frac{W}{g} \frac{\Delta V}{I_{sp}} \quad (3)$$

The spacecraft will pass 2 nodal points per day or (361)/ (2) = 730 nodal passes/year. The total impulse to be delivered at each nodal point is thus (I/730), or

$$i_n = \frac{1}{730} \frac{W}{g} \Delta V \quad (4)$$

Thus each of the two thrusters must provide this total impulse daily.

With the above relation one can now examine several cases of interest:

Case 1 - Thrust level fixed a a value of T.

Once the thrust level is fixed one has automatically fixed the total firing time τ or the number of degrees about each node, that will produce the required impulse at the node. This firing time (τ) in hours is thus

$$\tau_2 = \frac{i_n}{3600T} = \frac{1}{(730)(3600)} \frac{W}{g} \frac{\Delta V}{T} \quad (5)$$

Since the rate of change of spacecraft position is 15 degrees per hour, the total number of degrees of thruster firing about a node to deliver the required total impulse is thus

$$\theta_s = \frac{15°}{(730)(3600)} \frac{W}{g} \frac{\Delta V}{T} \quad (6)$$

The corresponding total system bus power required is $P_t = T/_{(T/P)}\eta$ with T/P the thrust/power ratio of the thruster (T is lb_f and P in kw) and η is the power conditioning efficiency.

Case 2:

a) <u>The impulse is to be delivered in the time interval τ_s</u>

From equation (5) one finds the required thrust level to be

$$T = \frac{1}{730}\,\frac{1}{3600}\,\frac{W}{g}\,\frac{\Delta V}{\tau_s} \tag{7}$$

and the corresponding total bus power level of operation

$$P = T/\eta\,(T/P) = \frac{1}{730}\,\frac{1}{3600}\,\frac{W}{g}\,\frac{1}{\eta}\,\frac{\Delta V}{\tau_s\,(T/P)} \tag{8}$$

when T is in lb_f and P in kw.

b) <u>The impulse is to be delivered over θ_s degrees:</u>

In this case the thrust level of operation is automatically defined. The value of thrust that must be provided is thus:

$$T = \frac{15^\circ}{(730)\,(3600)}\,\frac{W}{g}\,\frac{\Delta V}{\theta_s} \tag{9}$$

If the thrust/power ratio (T/P) is known, the required total system bus power level is thus:

$$P = \frac{T}{\eta\,(T/P)} \tag{10}$$

where T is in lb_f and P in kw.

The accuracy of the calculation decreases as θ increases.

Case 3: Power level of Operation is Fixed

This constraint lends itself to meaningful calculations only if the thrust/power ratio of the system is known. Once (T/P) is known one immediately defines the (maximum) thrust level of operation, i.e., T = P (T/P) and calculations can be carried out as for Case 1. i.e.,

$$\tau_s = \frac{1}{(730)\,(3600)} \quad \frac{W}{g} \quad \frac{\Delta V}{P\,\eta\,(T/P)} \tag{11}$$

and

$$\theta_s = \frac{15}{(730)\,(3600)} \quad \frac{W}{g} \quad \frac{\Delta V}{\eta\,P\,(T/P)} \tag{12}$$

The total number of thruster firings of each thruster during the mission life is thus:

$$n = i/i_b = \frac{A}{2i_b} \quad \frac{W}{g} \quad \Delta V \tag{13}$$

with i_b the impulse bit amplitude per thruster firing.

The pulse frequency (f) during any cycle of thruster operation is thus:

$$f = \frac{T}{i_b} \tag{14}$$

Several observations can be made regarding the selection of a pulsed plasma propulsion system to meet a particular mission requirement. Simple considerations show that a trade-off exists between the propulsion system weight and its reliability for performing the mission. The propulsion system weight is comprised of certain fixed weights and the weights that are a function of discharge energy. Both the specific impulse and the capacitor weight are known to be functions of discharge energy. Figure A-1 schematically depicts propellant, capacitor and the fixed weight as a function of discharge energy for a system capable of delivering a fixed total impulse. Furthermore, the total weight is also shown.

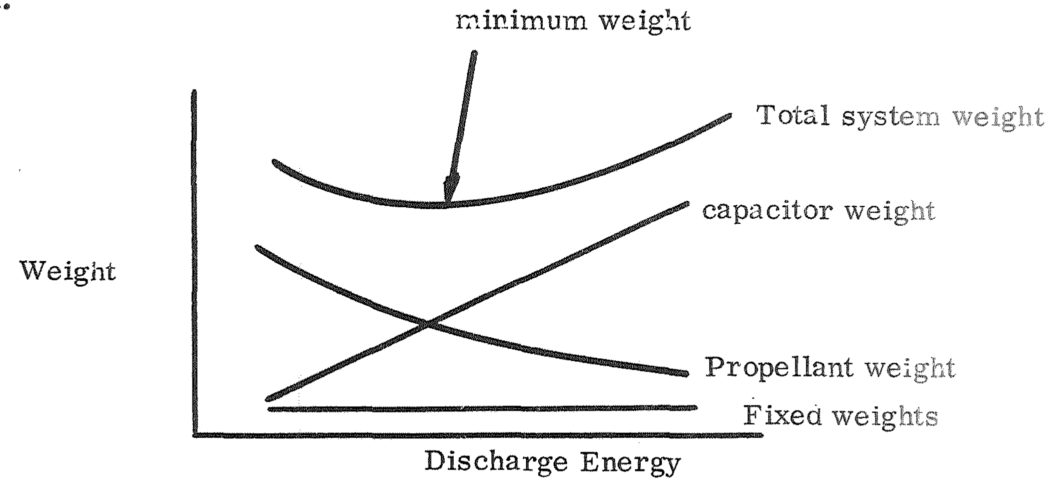

Figure A-1. Weight as a Function of Discharge Energy

For a system capable of delivering a certain total impulse and operating at some fixed power level, there exists one configuration having minimum weight. This minimum weight configuration requires that the system use a capacitor having a particular value of discharge energy. Configurations having a higher discharge energy will generally be more reliable. However, this increased reliability is had at the expense of increased total system weight. Changing either the total impulse capability or the power level of operation will change the required discharge energy level of operation for minimum total system weight.

PART II - SPINNING SATELLITES

In general, all of the relations of Part I are also applicable for spinning satellites. However, an additional constraint is imposed if the location of one or more thrusters on the satellite and the direction of the spin axis relative to the orbit plane is such that any one thruster can fire at most only once per spacecraft revolution to perform either the North or the South stationkeeping function. This additional constraint automatically defines the pulse frequency of thruster operation and also the amplitude of each impulse bit (i_b) to be delivered.

The average overall thrust level T (in lbs) that must be delivered to perform stationkeeping is related to propulsion system firing frequency, the satellite spin rate and the impulse bit amplitude (i_b in lbf-sec) of each discharge as

$$T = \frac{\omega}{60} \quad \frac{\alpha}{\beta} \quad i_b \tag{15}$$

with ω the satellite spin rate in rpm, α the number of thrusters to be used to perform the stationkeeping function (α = 1, 2, ...) and β to take into account that if one thruster is used (i.e., α =1) it may be discharged once every β revolution (β = 1, 2, 3....)

A general expression for the system power can also be readily presented. In general the power going into the capacitors will be

$$P_c = \frac{\omega}{60} \quad \frac{\alpha}{\beta} \quad E_d$$

with E_d the energy (joules) of each discharge. Now,

$$E_d = \frac{i_b}{i_b / E_d}$$

where i_b / E_d of a given thruster is numerically equal to its thrust/power ratio (in appropriate units). Hence,

$$P_c = \frac{\omega}{60} \quad \frac{\alpha}{\beta} \quad \frac{i_b}{(i_b / E_d)} \tag{16}$$

with i_b in lb_f-sec, E_d in joules and P_c in watts. If η denotes the power conditioning efficiency the overall bus power P_t becomes

$$P_t = \frac{P_c}{\eta} = \frac{\omega}{60} \quad \frac{\alpha}{\eta \beta} \quad \frac{i_b}{(i_b / E_d)} \tag{17}$$

Expressions corresponding to those presented for the 3 cases for 3-axes stabilized satellites can now be presented for spinning satellites:

Case 1: Thrust Level Fixed at a Value T

Fixing the overall thrust level also automatically fixes the impulse bit amplitude of each discharge of each of the α number of thrusters. From Equation 15:

$$i_b = \frac{60\beta}{\omega\ \alpha}\ T \qquad (18)$$

The system firing duration τ s and θ s are also given by Equations 5 and 6, respectively, with the overall thrust T being the input value. The system bus power is given by Equation 17 with i_b determined by Equation 18.

Case 2: a) The Impulse to be delivered over θ, degrees

The systems thrust level is determined by Equation 7 with the amplitude of each discharge given by Equation 18. The corresponding total bus power can then be evaluated from Equation 17.

b) The impulse to be delivered in the interval of time τs

Equation 9 defines the required thrust level of operation. The amplitude of each impulse bit will then be defined by Equation 18. Total system bus power can then be evaluated for Equation 17.

Case 3: Power Level of Operation is Fixed

Defining total system bus power automatically defines the impulse bit amplitude (i_b) to be provided by each discharge. From Equation 17 one finds

$$i_b = \frac{60\ \eta\ \beta\ \ (ib/Ed)}{\omega\ \alpha}\ P_t$$

Further calculations can then be carried out as for Case 3 of Part I.

Case 4: Impulse Bit Amplitude Fixed

For structural reasons it may, in some cases, be desirable to limit the amplitude of each impulse bit. In such cases one can either limit the system thruster level to a value defined by Equation 15, or adjust the number of thrusters (α) to provide any desirable thrust level.

The total number of discharges n_d that the propulsion system must provide over a mission life of A years in which I lb-sec of total impulse is produced (See Equation 1) is also found from Equation 13.

Case 5: Extremely Slow Spin Rate

In the special case where the satellite rotation is very slow, it may be desirable to discharge the thruster twice about the desired firing direction i.e., θ° before and θ° after the desired direction. The effective impulse bit amplitude is then $2I \cos \theta$. The available charge time per discharge will be $\theta / 3\omega$ sec (with ω in rpm and θ in degrees). The effective thrust level is:

$$\frac{\text{Total effective impulse}}{\text{Spin Period}} = \frac{2I \cos \theta}{60/\omega} = \frac{I \omega \cos \theta}{30}$$

and the average power consumed during the charge cycle will be:

$$P_{av} = \frac{E_d}{\theta / 3\omega} \qquad \frac{3\omega E_d}{\theta}$$

while the average power during a thrusting cycle becomes:

$$P_c = \frac{2E_d}{60/\omega} = \frac{\omega E_d}{30}$$

Example:

Suppose $W = 2000$ lb, $\omega = 10$ rpm, $\Delta V = 160$ ft/sec/year and each impulse bit is 3×10^{-3} lb sec. The average thrust level is thus $I/\tau = 500\ \mu$ lb. If the thrust/power ratio is $6\ \mu$ lb/watt, then $P = 500/6 = 83.4$ watts. With a power conditioning efficiency of 0.9, the bus power becomes $83.4/0.9 = 92.6$ watts. The impulse to be delivered per node is (2000/32.2) (160) (1/730) = 13.6 lb-sec. Hence the number of pulses/node equals $13.6/3 \times 10^{-3} = 4530$. Since the spin period is 6 seconds a total of 7.58 hours will elapse before the required impulse is delivered. If the total mission requires 30,000 lb-sec of total impulse, the thruster must provide a total of $30{,}000/3 \times 10^{-3} = 10 \times 10^{6}$ pulses.

The above considerations assumed ΔV to be a constant. This assumption implies that the impulse should be delivered at the node.[16] Since the entire impulse is not delivered at the node by the pulsed plasma propulsion, a correction to the ΔV requirements must be made. Using the data from Ref. 17, one can approximate the latter data by the empirical expression:

$$\Delta V = 150\ (1+3.6\times10^{-3} t^{2}) \quad \text{ft/sec-year}$$

with t the thrusting time in hours. For increased accuracy one can rederive all of the expressions presented using the empirical expression for ΔV.

APPENDIX B

CORRELATION OF SPECIFIC IMPULSE WITH PARAMETER $\int i^2 dt/m$

The simplified analysis presented in Section 3.2.2.1 suggested a relationship between the parameter $\int i^2 dt/m$ and propellant specific impulse. Available data of short pulse and quasi-steady operation is presented in Figure 28. The data presented shows that a reasonably good correlation exists between these two parameters. It is interesting to note that the quasi-steady data falls along a different trend line than short pulse discharge data. It is seen that at a given specific impulse the parameter $\int i^2 dt/m$ of short pulse operation is several times larger than the value evaluated for quasi-steady thruster operation. Malliaris[7] has found in his quasi-steady studies that erosion is severe above a critical value of $j^2/\dot{m}$. The results of the present study showed that the short pulse discharge thruster could operate with little erosion at values of $\int i^2 dt/m$ corresponding to a region of severe erosion for quasi-steady operation. The present results would therefore suggest that the regime for the onset of severe erosion is different for both types of operation.

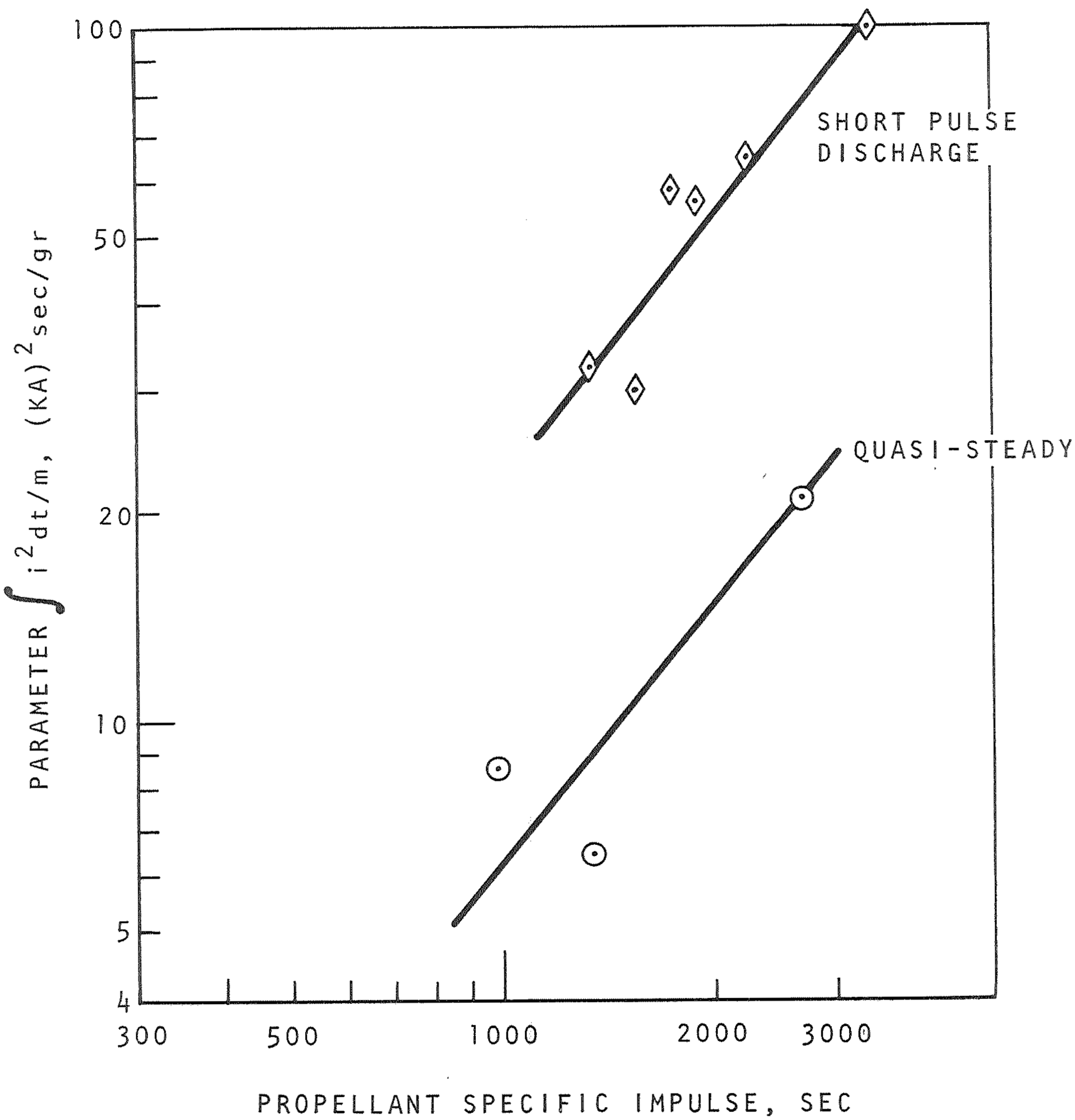

Figure 28. Parameter $\int i^2 dt/m$ as a function of Propellant Specific Impulse

NASA CR-111935

DISTRIBUTION LIST
NAS1-9925

	No. Copies
NASA Langley Research Center Hampton, VA 23365 Attention: Program Reports & Analysis Unit, Mail Stop 122	1
Raymond L. Zavasky, Mail Stop 110	1
James M. Hoell, Jr., Mail Stop 160	10
NASA Ames Research Center Moffett Field, CA 94035 Attention: Library, Mail Stop 202-3	1
NASA Flight Research Center P. O. Box 273 Edwards, CA 93523 Attention: Library	1
Jet Propulsion Laboratory 4800 Oak Grove Drive Pasadena, CA 91103 Attention: Library, Mail 111-113	1
Dr. Noble M. Nerheim, Mail 122-123	1
NASA Manned Spacecraft Center 2101 Webster Seabrook Road Houston, TX 77058 Attention: Library, Code BM6	1
NASA Marshall Space Flight Center Huntsville, AL 35812 Attention: Library	1
Ernst Stuhlinger, AD-S	1
NASA Lewis Research Center 21000 Brookpark Road Cleveland, OH 44135 Attention: Library, Mail Stop 60-3	1
Wolfgang E. Moeckel, Mail Stop 301-1	1
George R. Seikel, Mail Stop 301-1	1
NASA Goddard Space Flight Center Greenbelt, MD 20771 Attention: Library	1
William C. Isley, Code 734	1
John F. Kennedy Space Center Kennedy Space Center, FL 32899 Attention: Library, Code IS-DOC-12L	1
National Aeronautics & Space Administration Washington, DC 20546 Attention: Library, Code KSS-10	1
NASA Code RP	1
James Lazar, Code KSS-10	1
Jerome P. Mullin, Code RNT	1

DISTRIBUTION LIST
NAS1-9925

	No. Copies
Comsat Laboratories Positioning & Orientation Branch Washington, DC 20013 Attention: Bernard Free	1
Princeton University Guggenheim Laboratories James Forrestal Campus Princeton, NJ 08540 Attention: Woldemar F. von Jaskowsky	1
TRW Systems Inc. One Space Park Redondo Beach, CA 90278 Attention: Dr. C. L. Dailey	1
Air Force Weapons Laboratory Kirtland Air Force Base, NM 87417 Attention: WLPC/Capt. C. F. Ellis	1
Thermal Mechanical Research Laboratory OAR USAF Wright-Patterson Air Force Base, OH 45433 Attention: Eric Soehngen	1
Catholic University of America Department of Space Sciences & Applied Physics Washington, DC 20017 Attention: Professor C. C. Chang	1
General Electric Company Missile & Space Division Space Sciences Laboratory P. O. Box 8555 Philadelphia, PA 19101 Attention: Dr. Thomas W. Karras	1
Los Alamos Scientific Laboratories P. O. Box 1663 Los Alamos, NM 87544 Attention: Dr. Stratton	1
AVCO Corporation Research & Advanced Development Division 201 Lowell Street Wilmington, MA 01887 Attention: A. C. Malliaris	1
University of California, San Diego LaJolla, CA 92037 Attention: Professor R. Lovberg	1

DISTRIBUTION LIST

NAS1-9925

	No. Copies
Research and Technology Division Wright-Patterson Air Force Base, OH 45433 Attention: David Fritts, AFAPL (APIE-1)	1
United States Air Force Office of Scientific Research Washington, DC 20025 Attention: M. Slawsky	1
Princeton University Forrestal Research Center Princeton, NJ 08540 Attention: Dr. R. G. Jahn	1
Giannini Scientific Corporation 3839 South Main Street Santa Ana, CA 92702 Attention: Adriano Ducati	1
NASA Scientific & Technical Information Facility P. O. Box 33 College Park, MD 20740	7 plus reproducible